




Cite this: *Soft Matter*, 2021,  
17, 3533

Received 1st October 2020,  
Accepted 18th January 2021

DOI: 10.1039/d0sm01758b

[rsc.li/soft-matter-journal](http://rsc.li/soft-matter-journal)

## More than just a barrier: using physical models to couple membrane shape to cell function

Felix Frey  and Timon Idema \*

The correct execution of many cellular processes, such as division and motility, requires the cell to adopt a specific shape. Physically, these shapes are determined by the interplay of the plasma membrane and internal cellular driving factors. While the plasma membrane defines the boundary of the cell, processes inside the cell can result in the generation of forces that deform the membrane. These processes include protein binding, the assembly of protein superstructures, and the growth and contraction of cytoskeletal networks. Due to the complexity of the cell, relating observed membrane deformations back to internal processes is a challenging problem. Here, we review cell shape changes in endocytosis, cell adhesion, cell migration and cell division and discuss how by modeling membrane deformations we can investigate the inner working principles of the cell.

### 1 Introduction

Cellular processes such as endocytosis, cell adhesion, cell migration and cell division depend crucially on the ability of cells to adapt and control their shape. The shape of a cell is determined by its complex internal structure. Eukaryotic cells are surrounded by a plasma membrane that forms a barrier and separates the cell's interior from its environment.<sup>1</sup> Contained within this barrier is the cytoskeleton, a dynamical scaffold of different polymer networks that organizes cell shape.<sup>2,3</sup>

In order to determine the driving factors that control cell shape and reduce the system's complexity, a rewarding approach is to simplify the system by reconstituting it "bottom up", with the ultimate goal of building a synthetic cell.<sup>4,5</sup> One of the aims of such a reductionist approach is to disentangle the mechanisms and contributions of the different intracellular processes.<sup>6</sup> However, to experiment with a complex system, like a cell, is technically challenging, even when considering a simplified version. Therefore, it is helpful to take complementary approaches.

Already back in 1917 D'Arcy Thompson suggested in his book *On Growth and Form* that the shape of biological organisms, including cells, is determined by physical forces.<sup>7</sup> Using this idea

*Department of Bionanoscience, Kavli Institute of Nanoscience, Delft University of Technology, Delft, The Netherlands. E-mail: T.Idema@tudelft.nl*



**Felix Frey**

*concerned with the application of concepts from soft matter physics to biophysics and is focused on assembly processes and interactions between the plasma membrane and the cytoskeleton.*

*Felix Frey studied Physics at Heidelberg University and earned his PhD at Heidelberg University in 2019 in the group of Ulrich Schwarz at the Institute for Theoretical Physics. During his PhD he worked on uptake processes at the plasma membrane such as virus particle uptake and clathrin-mediated endocytosis. He then joined Timon Idema's group at the Department of Bionanoscience at TU Delft as a postdoctoral fellow. His work is*



**Timon Idema**

*interactions and emergent phenomena in systems of many active particles. Next to his research work, he is very active in education, for which he received the J. B. Westerdijkprize in 2020.*

*Timon Idema studied Physics and Mathematics at Leiden University and earned his PhD at Leiden University in 2009. He then worked as a postdoctoral researcher at the University of Pennsylvania. In 2012 he became assistant professor at TU Delft where he started a theoretical biophysics group. Since 2018 he is an associate professor. He is interested in soft matter physics and biophysics with a particular interest in membrane-mediated*



in reverse, it is also possible to determine intracellular forces and processes that lead to a particular shape by examining the cell shape and the dynamics of shape changes. Since the plasma membrane surrounds the cell, it mirrors both the activity inside the cell and the response of the cell to its environment.<sup>8</sup> In particular, the plasma membrane is not static but highly dynamic because it is vital for the cell to be able to adapt its shape quickly.

Deformations appear in a huge variety because diverse driving factors frequently deform the membrane in various cellular processes.<sup>9</sup> Thus, both the shape and dynamics of deformations contain information about the generating forces and driving factors. Because cells are under osmotic pressure, due to differences in ion concentrations between the inside and outside of the cell, in solution they take on a spherical shape.<sup>3</sup> In the absence of external perturbations, the spherical shape therefore defines the reference shape with which all deformations are compared (*cf.* Fig. 1a). For instance, processes like membrane fluctuations, endocytosis, cell adhesion, cell migration, and cell division deform the plasma membrane in a characteristic manner compared to the spherical reference state (*cf.* Fig. 1b–f).

Observing shape changes and membrane deformations is relatively simple, because they act on a mesoscopic length scale ( $\sim \mu\text{m}$ ) and therefore are experimentally accessible. This makes it possible to determine either the membrane properties or the cellular functions. While the investigation of passive membrane fluctuations makes the membrane properties measurable, the investigation of membrane deformations in processes such as active membrane fluctuations, endocytosis, cell adhesion, cell migration or cell division provides information

about cell functions. The challenge is then to infer the driving forces from membrane deformations. While we go through the different examples (*cf.* Fig. 1), we also review various modeling strategies. These strategies include both continuum and discrete models. Examples of the first type consider cytoskeletal networks as fields of active fluids or liquid crystals, whereas examples of the second type consider ligand–receptor contacts as discrete binding sites or triangulate the membrane. In addition to these approaches, particle based coarse-grained molecular dynamics simulations are used to study the shape and dynamics of membranes, for example to investigate how membrane-bound protein clusters deform the membrane during assembly.

This review is structured as follows: In Section 2 we give a short biophysical background on the plasma membrane and the cytoskeleton, which are the two main determinants of cell shape. We then introduce the central modeling concept, the Helfrich Hamiltonian, which forms the basis for most of the membrane models that we discuss. In Section 3 we discuss how thermal and active fluctuations impact cell shape, while in Sections 4–7 we investigate what can be learnt by modeling membrane deformations in endocytosis, cell adhesion, cell migration and cell division. In Section 8 we conclude by a discussion of future challenges and open questions. In particular, we highlight throughout the review how modeling membrane deformations is an important tool to investigate the inner workings of the cell.

## 2 Defining cell shape: the plasma membrane and the cytoskeleton

### 2.1 Biophysical background

The shape of the cell is largely determined by the plasma membrane and the cytoskeleton.<sup>1,2</sup> Since the plasma membrane separates the cell from its environment, it mirrors the activity within the cell, but also indicates the response of the cell to its surroundings. Compared to the dimensions of a cell ( $\sim 30 \mu\text{m}$ ), the plasma membrane is relatively thin ( $\sim 4 \text{ nm}$ ). The plasma membrane is a fluid lipid bilayer, made of different lipid molecules with hydrophobic tails and hydrophilic heads, in which diverse proteins are embedded (*cf.* Fig. 2a).<sup>1,9</sup> The plasma membrane is supported by the underlying actin cortex, which is around 100 nm thick and made of a layer of branched and crosslinked actin filaments.<sup>10,11</sup> Although the plasma membrane is anchored to the actin cortex by linker molecules of the ERM family (ezrin, radixin, moesin), it can still fluctuate due to the large distances of 10–20 nm between the membrane and the cortex.<sup>12,13</sup> Other important protein classes that are embedded in the plasma membrane are ion pumps (transporters that actively shuttle ions across the membrane) and ion channels (gates that are either open or closed). Since they pump water out of the cell and modulate ion concentrations within the cell, they ensure that the osmotic pressure is neither too low nor too high.<sup>3</sup> Because of their activity, they also exert forces on the membrane.

In addition to these forces generated by ion pumps and channels, the cytoskeleton can also exert forces that deform

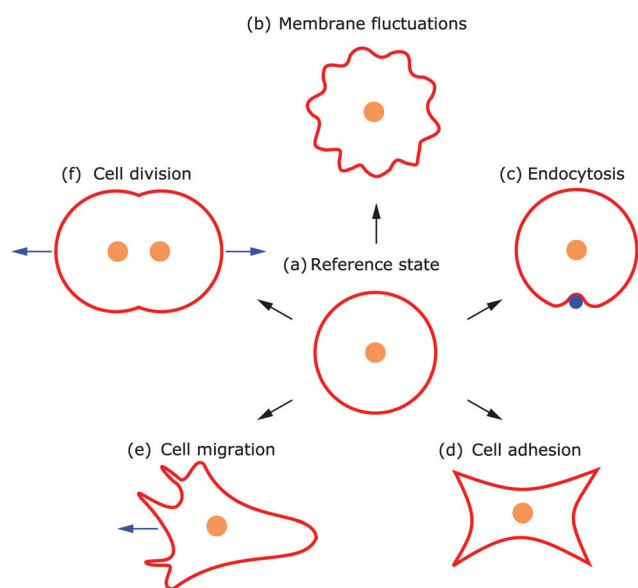


**Fig. 1** Examples of different cell shapes, directly related to the underlying cellular processes. (a) In its undeformed reference state the cell assumes a spherical shape. Different processes lead to typical cell shapes deforming the plasma membrane due to (b) membrane fluctuations, (c) endocytosis, (d) cell adhesion, (e) cell migration, and (f) cell division.



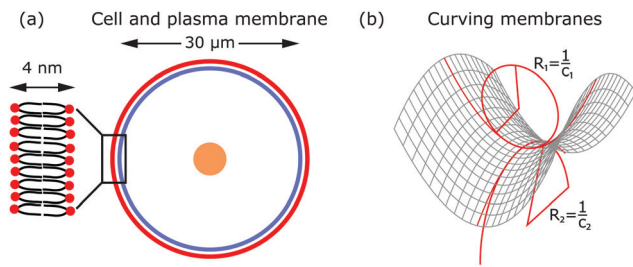


**Fig. 2** The biophysical properties of the plasma membrane. (a) The plasma membrane (red) surrounds the cell with nucleus (orange). The membrane is supported by the actin cortex (blue). Inset: The membrane is a fluid lipid bilayer of phospholipids with hydrophobic tails (black) and hydrophilic heads (red). (b) The plasma membrane can be modeled as a 2D surface in 3D space. Two principal curvatures (shown by two fitted circles with different radii) describe the deformation of the membrane at every point.

the membrane. The cytoskeleton is a composite meshwork, made of polymer networks, crosslinker proteins and molecular motors. The three main components building up the polymer networks are actin filaments, microtubules and intermediate filaments.<sup>14</sup> In addition, septin filaments have been described as another cytoskeletal component that can assemble into hierarchical structures, sense membrane curvature and, hence, stabilize membrane deformations (as for example in cell division).<sup>15,16</sup> Of particular interest in this context are actin filaments and molecular motors, because together they are probably the most important sources that generate active membrane deformations.<sup>17</sup>

Actin filaments grow by the addition of actin monomers. The growth mainly happens at the plus (or barbed) end, where ATP-actin, *i.e.* monomers to which ATP is bound, attaches, after which the ATP is hydrolyzed. Thus, the growth of actin filaments is an active process.<sup>10</sup> Actin filaments can organize into adaptive higher-order structures of various architectures such as parallel bundles or branched networks.<sup>17</sup> Depending on the architecture of the growing actin network, different cell shapes and membrane deformations evolve. For example in phagocytosis and cell migration the plasma membrane gets deformed by the growth of branched actin networks.

Polymerizing actin structures and contractile ones are both able to deform the plasma membrane.<sup>18</sup> The contraction of actin networks is caused by molecular motors that consume energy by hydrolyzing ATP.<sup>17</sup> Myosin molecular motors form a protein family that is associated with actin filaments. Myosin II motors can assemble and form myosin II mini-filaments, which are able to contract branched or bundled actin networks. For instance, in cell migration the membrane is deformed due to polymerizing actin filaments at the front of the cell while the back of the cell is contracted by actin stress fibers (crosslinked and contractile actin bundles). In contrast, in cell division the membrane is deformed due to the contracting actin cortex.

Deformations of the plasma membrane can be caused by both passive and active processes. Membrane deformations caused by passive processes either occur in equilibrium or drive the system towards equilibrium, *i.e.*, they minimize the free

energy of the system, without additional energy consumption. Examples are membrane fluctuations due to thermal random kicks of the surrounding medium, endocytosis driven by adhesion or the assembly of protein superstructures. Moreover, membrane deformations and fluctuations can be driven by active processes. Following the usual definition, active processes consume energy, *i.e.*, they run out of equilibrium and are capable of converting free energy into systematic activity.<sup>19–21</sup> Examples of such processes are active membrane fluctuations, phagocytosis, cell migration and cell division. Here, the activity originates for instance from ion channels or pumps, growing and contracting actomyosin or septin networks, and other protein families such as clathrin, caveolin-1 or ESCRT-III.<sup>15,17,22,23</sup>

## 2.2 Modeling deformations of the plasma membrane: the Helfrich Hamiltonian

From a physical point of view the plasma membrane can be modeled as a surface in three-dimensional space that is described locally by its two principal curvatures  $C_1$  and  $C_2$  (*cf.* Fig. 2b). The usual starting point for continuum models describing membrane deformations is the Helfrich Hamiltonian.<sup>24</sup> The Helfrich Hamiltonian describes the elastic energy of the plasma membrane, with the most relevant contribution being the out-of-plane bending energy. In contrast, the shear modulus vanishes due to the fluid nature of the lipid bilayer.<sup>25</sup> Because the lipids of the membrane are closely packed, the compression modulus is large, and thus the contribution from compression is also negligible. In addition, there is an entropic contribution to the free energy of the plasma membrane, quantifying the energetic cost to pull out excess area as for instance membrane fluctuations, effectively acting as a tension energy. Hence, the free energy of the membrane reads

$$\mathcal{H} = 2\kappa \int (H - H_0)^2 dA + \sigma \int dA + \bar{\kappa} \int K dA, \quad (1)$$

where  $H = 1/2(C_1 + C_2)$  is the mean curvature,  $H_0$  is the spontaneous (mean) curvature of the membrane resulting from any asymmetry in the bilayer, and  $K = C_1 C_2$  is the Gaussian curvature.<sup>25</sup> The membrane's material parameters are the bending rigidity  $\kappa$  and the saddle-splay (or Gaussian) modulus  $\bar{\kappa}$ . The tension  $\sigma$  can be interpreted either as the chemical potential for membrane area quantifying the energetic cost to pull out excess area, or as a Lagrange multiplier to constrain the membrane area.<sup>25</sup> For any processes that do not involve topological changes (as *e.g.* fusing or splitting cells), the term containing the Gaussian curvature is constant due to the Gauss–Bonnet theorem and thus can be neglected.<sup>25</sup> When the volume enclosed within the membrane is fixed, a term  $\Delta p \int dV$ , with  $\Delta p$  the pressure difference between inside and outside, is added to eqn (1).

An alternative description to the Helfrich Hamiltonian or spontaneous curvature model is the bilayer-couple model that assumes fixed but different numbers of lipids in the inner and outer monolayers of the membrane and thus different monolayer areas.<sup>26,27</sup> The resulting energy functional is similar to eqn (1) without including a contribution from spontaneous



curvature. The approach can be extended in the Area Difference Elasticity (ADE) model where one assumes that the monolayers can also stretch.<sup>26,28</sup> In this case one finds an energy functional identical to eqn (1) but now also including a stretching energy term that takes the area difference between the monolayers into account. Although the ADE model describes transitions of membrane shapes more accurately,<sup>27,28</sup> for simplicity most authors use the Helfrich Hamiltonian, as we will do in the following.

In equilibrium, the shape of the plasma membrane is the one that minimizes its energy. To find this equilibrium shape, we calculate the variation of eqn (1) with respect to the membrane shapes, which gives us the shape equation of the membrane, akin to the Euler–Lagrange equation for the action in classical mechanics. In its general form (now including  $\Delta p$ ) the shape equation reads<sup>29</sup>

$$\Delta p - 2\sigma H + \kappa(2H + 2H_0)(2H^2 - 2K - 2H_0H) + 2\kappa\Delta H = 0. \quad (2)$$

While for most geometries the shape equations are non-linear partial differential equations, for simple geometries with rotational symmetry the equations simplify to non-linear ordinary differential equations. For vanishing bending rigidity ( $\kappa = 0$ ) the shape equation simplifies to  $\Delta p = 2\sigma H$ , which is the Laplace law, for example governing the shape of soap bubbles. By solving the shape equation, shapes similar to membrane vesicles or red blood cells can be determined dependent on the different model parameters (as *e.g.* reduced volume  $\nu$ , that is the ratio between the vesicle volume and the area-equivalent spherical volume, see eqn (15)).<sup>30–32</sup> For example, a floppy vesicle with  $\nu = 0.592–0.651$  and  $H_0 = 0$  has an oblate shape.<sup>31</sup> Inversely, the membrane parameters can be inferred from fitting membrane shapes.<sup>33,34</sup> However, more accurate values for these parameters can be obtained in other experiments, for example from measurements of the membrane fluctuation spectrum (see Section 3), or by pulling membrane tubes from large vesicles. For the latter case, by measuring the applied pulling force, either the membrane tension or the bending rigidity can be calculated if the other parameter is known.<sup>35–37</sup>

To conclude, by modeling plasma membranes, using the framework of the Helfrich Hamiltonian in eqn (1), it is possible to predict equilibrium membrane shapes and thus the shapes of simple biological cells such as red blood cells, and to relate membrane shapes to measurable material properties.

### 3 Membrane fluctuations

The plasma membrane is always affected by fluctuations, which cause transient deformations that survive for only a short period of time ( $\sim 1–10^4$  ms). Originally they were thought to be generated by thermal noise only, however, today we know that there are also several active origins that could drive membrane flickering, as reviewed by Turlier and Betz.<sup>22</sup> Fig. 3a shows the spherical reference state (dashed) and a

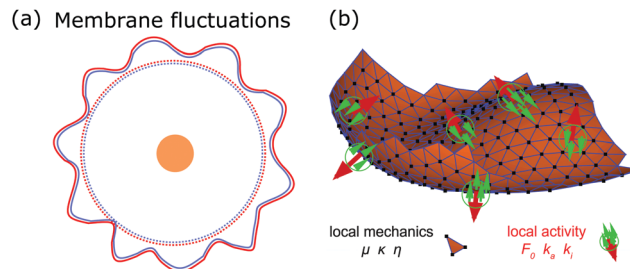


**Fig. 3** Membrane deformations due to fluctuations of various origins. (a) Schematics of membrane fluctuations, caused by thermal random kicks from the environment, ion channels, ion pumps, and the coupling of plasma membrane and cytoskeleton. The spherical reference state of the cell (dashed) and a deformed state (solid) are shown. Membrane: red, actin cortex: blue and cell nucleus: orange. (b) Simulation snapshot of a triangulated membrane exhibiting active fluctuations. The mechanical properties of the membrane and the surrounding fluid are represented by the shear modulus  $\mu$ , the bending rigidity  $\kappa$  and the fluid viscosity  $\eta$ . The forces with amplitude  $F_0$  are activated and inactivated with rates  $K_a$  and  $K_i$  and deform the membrane (red arrows). The surrounding fluid counteracts the active forces (green arrows). Reproduced from ref. 44 with permission from Springer Nature, copyright (2016).

deformed state (solid) of the plasma membrane (red) and the actin cortex (blue) due to fluctuations of various origins.

First, thermal random kicks of the surrounding medium drive membrane fluctuations.<sup>38</sup> Second, and roughly equally important, several active processes drive membrane fluctuations, including the action of ion pumps and ion channels. Both pumps and channels can generate ion gradients and electric potentials that help the cell to control osmotic pressure and excitability. At the same time, as a consequence of Newton's third law, they exert additional forces onto the membrane, that lead to active fluctuations.<sup>22</sup>

By investigating membrane fluctuations, both the elastic properties of the plasma membrane and the possible active origin of the fluctuations can be studied. Membrane fluctuations are most easily characterized in red blood cells, since red blood cells lack a nucleus and thus represent a simple experimental model system. In red blood cells the actomyosin cortex and the spectrin network (another polymer network attached to the membrane) introduce additional sources of activity, which exert forces onto the membrane and lead to active fluctuations.<sup>39,40</sup> The fluctuation spectrum of the membrane is typically observed with video microscopy or fluctuation spectroscopy. The elastic properties of the membrane such as the membrane tension or bending rigidity can then be determined by fitting the fluctuation spectrum.<sup>38,41,42</sup> Moreover, by fitting membrane shapes to simulated triangulated surfaces the spontaneous curvature of the membrane can be determined as well.<sup>43</sup> In addition, differences between the measured fluctuation spectrum and the prediction of the spectrum for purely thermally driven fluctuations suggest that the fluctuations are driven by active processes.<sup>44</sup> For example, the time scale for thermally or actively induced fluctuations differs. While thermally induced fluctuations act on all time scales, actively induced fluctuations mostly enhance the amplitude for



fluctuations acting on the time scale of  $10^2$ – $10^4$  ms. In the following sections, we discuss how passive and active membrane fluctuations can be modeled.

### 3.1 Passive fluctuations

Because the plasma membrane is always affected by thermal fluctuations, a background of membrane deformations develops, which gives rise to a whole spectrum of membrane fluctuations. Since membrane fluctuations deform the plasma membrane only weakly, it is useful to describe the membrane by a height function  $h(x,y)$ , that is a scalar field of the internal membrane coordinates  $x$  and  $y$ . This parametrization of membrane shape is known as the Monge gauge.<sup>45</sup> For small deformations, we can expand eqn (1) to second order in  $h$  and its derivatives:

$$\mathcal{H} = \frac{\kappa}{2} \int (\Delta h)^2 dx dy + \frac{\sigma}{2} \int (\nabla h)^2 dx dy, \quad (3)$$

where the infinitesimal area element was expanded as  $dA = (1 + 1/2(\nabla h)^2) dx dy$ . As the plasma membrane is deformed on various length scales, it makes sense to expand eqn (3) in Fourier modes since the corresponding wave vectors  $q$  decouple. In this way the different deformation length scales are separated and we get

$$\mathcal{H} = \frac{1}{2} \int (\kappa q^4 + \sigma q^2) h(q) h^*(q) q dq. \quad (4)$$

Applying the equipartition theorem, every Fourier mode  $q$  carries an energy of  $k_B T/2$ , which leads to the fluctuation spectrum<sup>46</sup>

$$\langle |h_q|^2 \rangle = \frac{k_B T}{\kappa q^4 + \sigma q^2}. \quad (5)$$

Eqn (5) connects the amplitude of a membrane fluctuation at a given Fourier mode with  $\kappa$  and  $\sigma$ . By fitting the fluctuation spectrum, the values of these parameters can be determined with high accuracy.

For passive systems the main driver of membrane fluctuations are random thermal kicks of the surrounding fluid. Thus, in order to describe the dynamics of the membrane and the fluid, the Navier–Stokes equation has to be coupled to eqn (3). The emerging Langevin equation then governs the dynamics of membrane deformations.<sup>47–49</sup> Because we are mostly interested in the behavior for low Reynolds numbers, we can neglect inertia, and the fluid is represented by the Stokes equation

$$\eta \Delta \mathbf{v}(\mathbf{r}) - \nabla p(\mathbf{r}) = \mathbf{F}(\mathbf{r}), \quad (6)$$

where  $\eta$  is the viscosity of the fluid,  $\mathbf{v}$  the fluid flow field,  $p$  the pressure field and  $\mathbf{F}$  an external force field. Together with the continuity equation for an incompressible fluid,  $\nabla \cdot \mathbf{v} = 0$ , the equation can be formally solved by

$$\mathbf{v}(\mathbf{r}) = \int \Lambda(\mathbf{r}, \mathbf{r}') \mathbf{F}(\mathbf{r}') d\mathbf{r}', \quad (7)$$

where  $\Lambda(\mathbf{r}, \mathbf{r}') = 1/8\pi\eta |\mathbf{r} - \mathbf{r}'|$  is the Oseen tensor. By identifying the fluid velocity at the interface with the dynamics of  $h(x,y)$ ,

we arrive at a Langevin equation for the membrane height

$$\frac{\partial h}{\partial t} = \int \Lambda(\mathbf{r}, \mathbf{r}') \left( -\frac{\delta \mathcal{H}}{\delta h} - \zeta(\mathbf{r}', t) - f(\mathbf{r}', t) \right) d\mathbf{r}', \quad (8)$$

where  $\zeta(\mathbf{r}', t)$  is a Gaussian uncorrelated thermal random force and  $f(\mathbf{r}', t)$  represents active forces acting on the membrane. Based on eqn (8) the dynamics of the membrane can then be determined as a result of thermal fluctuations and active forces.

### 3.2 Active membrane fluctuations

In order to explain active processes, such as irreversible chemical reactions or active transport across the membrane, we have to go beyond the description given by equilibrium statistical physics. We can integrate activity into the membrane by either including an active force  $f(\mathbf{r}', t)$  in eqn (8) or by modifying eqn (3). Prost and Bruinsma treated the embedded proteins as two-state systems that can be either active or passive and either exert forces (due to momentum exchange with the surrounding fluid) or no forces on the membrane.<sup>47</sup> The additional forces then lead to a modified Langevin equation, predicting a modified fluctuation spectrum compared to the passive case. Following this approach, it has been theoretically shown that active membrane fluctuations are amplified in front of a wall.<sup>48</sup>

The effect of active proteins such as ion channels and ion pumps was explored in a series of papers.<sup>50–53</sup> It has been suggested that ion channels affect the diffusion behavior in membranes, for instance that over long timescales diffusivity is increased.<sup>50</sup> Moreover, the interplay between membrane undulations and ion pumps has been modeled, suggesting that membrane undulations travel with a velocity that is determined by the pump activity, that undulations are proportional to the inverse of the viscosity of the surrounding fluid, and that the statistical distribution of active membrane fluctuations is non-Gaussian.<sup>51–53</sup> The interplay between excess area contained in membrane fluctuations and tension has furthermore been explored theoretically by Loubet *et al.* for a membrane that is subject to active fluctuations caused by a force resulting from pushing, spontaneous curvature, or permeation.<sup>54</sup> They suggest that active fluctuations change the fluctuation spectrum and effect the relation between tension and excess area.

The growth, binding dynamics, and contraction of the cytoskeleton also lead to active membrane deformations. Interactions of the plasma membrane with the cytoskeleton, modeled as spring networks, suggest that the coupled cytoskeleton produces large membrane fluctuations that help to regulate membrane area,<sup>55</sup> that cytoskeletal defects<sup>56</sup> and the membrane–cortex bond density<sup>57</sup> influence the fluctuation spectrum, and that the dynamics of the cytoskeletal network alters the elastic properties of the membrane.<sup>58</sup>

At large scales, cells show a tendency to form wavelike or unstable membrane deformations. The emergence of these patterns can be understood in a system with a feedback loop between the recruitment of membrane-bound activators and increased actin polymerization. The resulting shapes



then depend on the induced spontaneous curvature of the activators.<sup>59–61</sup>

Active membrane fluctuations have been studied experimentally using various observation techniques.<sup>62</sup> It has been shown that membrane-embedded ion pumps increase shape fluctuations and excess area,<sup>63</sup> and decrease membrane tension<sup>64</sup> compared to the passive case. Moreover, the amplitudes of membrane fluctuations are reduced in red blood cells that are depleted of ATP<sup>65,66</sup> and changed in red blood cells that are infected by malaria parasites.<sup>67</sup> Additional insight into how activity can change membrane shapes was provided by the recent experimental observation and numerical simulation of lipid vesicles that enclose bacteria,<sup>68</sup> and lipid vesicles that contain active Janus particles.<sup>69</sup> Both studies theoretically predicted, in agreement with the experimental data, that the observed active membrane fluctuation spectrum shows increased amplitudes for deformations acting on long wave lengths compared to the passive fluctuation spectrum.

The work by Turlier and coworkers is an illustrative example on how cellular processes can be theoretically inferred from these membrane deformations.<sup>44</sup> By analyzing the red blood cell fluctuation spectrum, they showed that it deviates from what one would expect for a membrane in equilibrium, suggesting that active processes contribute to these membrane deformations. Analytical calculations and simulations of a triangulated membrane on which active forces act (*cf.* Fig. 3b), support this finding. However, the nature of the processes leading to these active forces remains elusive, since simulations with both monopole and dipole forces agree equally well with the data.

To conclude, while the analysis of passive membrane fluctuations can inform us about material properties of the membrane that would otherwise be difficult to measure with the same ease and precision, the extension to active membrane fluctuations also gives us insight into cellular functioning, since the changed fluctuation spectrum is due to active processes inside the cell.

## 4 Endocytosis

After membrane fluctuations, endocytosis is conceptually the simplest cellular process that causes membrane deformations. In endocytosis extracellular material is brought into the cell, or simply speaking the cell wraps a particle in its plasma membrane in order to take it up. Compared to the other examples discussed in this review, membrane deformations in endocytosis act on smaller length scales which makes it more challenging to access them experimentally, because with standard light microscopy we cannot resolve the relevant details of the membrane shape. Various modes of endocytosis occur in the cell. Here, we discuss the three main cases, namely adhesion driven particle uptake, clathrin-mediated endocytosis, and phagocytosis (*cf.* Fig. 4a, d and g).

### 4.1 Adhesion driven particle uptake

While various entry modes exist in the cell, such as clathrin-mediated endocytosis or caveolar endocytosis, arguably the

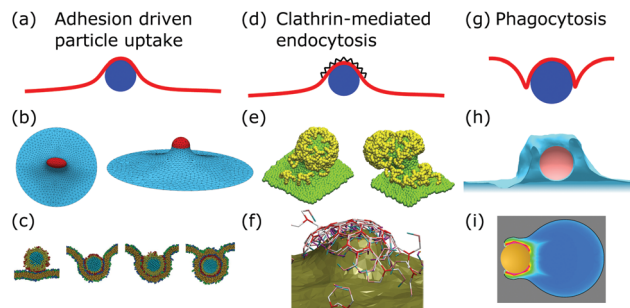


**Fig. 4** Membrane deformations in endocytosis. (a) Schematics of adhesion driven particle uptake. Membrane: red, particle: blue. (b) Simulated triangulated membrane, deformed by an adhered particle. Reproduced from ref. 80 with permission from The Royal Society of Chemistry. (c) Particle-based membrane simulation of particle uptake. Reproduced from ref. 91 with permission from Elsevier, copyright (2012). (d) Schematics of clathrin-mediated endocytosis. Membrane: red, particle: blue, clathrin lattice: black wedges. (e and f) Particle-based simulation of assembling clathrin triskelia deforming a membrane. (e) Reproduced from ref. 123 with permission from The Royal Society of Chemistry. (f) Reproduced from ref. 124 with permission from AIP Publishing. (g) Schematics of phagocytosis with the characteristic membrane deformation of the phagocytic cup. Membrane: red, particle: blue. (h) Simulation of particle engulfment in phagocytosis. Reproduced from ref. 128 with permission from Springer Nature, copyright (2010). (i) Simulation of engulfment of an antibody coated particle. The coloring shows the density of the actin cytoskeleton from blue (low) to red (high). Reproduced from ref. 129 under the terms of the Creative Commons Attribution License (CC BY 4.0).

simplest case of endocytosis is particle uptake driven by adhesion energy (*cf.* Fig. 4a). Examples include viruses and nanoparticles that are typically ten to several hundred nanometers large,<sup>70</sup> as well as micrometer-sized pathogens such as malaria parasites.<sup>71–74</sup> The adhesion energy, which the particle experiences upon making contact with the membrane, can be of various origins, including electrostatic interactions, ligand-receptor binding, and entropic, van der Waals, or hydrophobic forces.<sup>70</sup>

The uptake process starts if the energetic gain upon particle adhesion overcomes the energetic cost of bending the membrane and pulling out the excess area necessary to wrap the particle. Afterwards, adhesion driven uptake is an energetic downhill process that only stops if the energy minimum (*i.e.* a stable equilibrium) is reached. Since the connection of a fully wrapped particle to a membrane by means of a membrane neck costs approximately zero bending energy due to the saddle-shape of the neck ( $H = 0$  in eqn (1)), we immediately understand that after uptake, membrane scission has to be driven by an active process such as membrane constriction by dynamin.<sup>75,76</sup>

The adhesion process can be incorporated in our membrane model by adding the adhesion energy to eqn (1),

$$\mathcal{H} = - \int_{A_{\text{ad}}} W dA + 2\kappa \int (H - H_0)^2 dA + \sigma \int dA, \quad (9)$$

where  $W$  quantifies the adhesion energy density along the adhesive particle surface  $A_{\text{ad}}$ .<sup>75,77,78</sup> Note the minus sign in front of the first term, showing that adhesion is energetically favorable.



The main results of uptake models based on eqn (9) are that membrane tension, bending rigidity and adhesion strength determine whether one has full uptake, partial uptake or no uptake (*cf.* Fig. 4b).<sup>75,77,79–81</sup> For example, for an intermediate adhesion energy and low membrane tension one has full uptake, while for an intermediate adhesion energy and large membrane tension one has partial uptake. In general, the competition between adhesion energy and membrane tension determines if partial uptake occurs, while the competition between adhesion energy (dependent on particle size) and bending energy (independent of particle size) defines a critical particle radius  $\sqrt{2\kappa/W}$  below which uptake is not possible.<sup>78,82</sup> Uptake dynamics and membrane deformations are also studied for non-spherical particle shapes,<sup>79,81,83</sup> for particles with elastic properties,<sup>84,85</sup> for membranes with spontaneous curvature,<sup>86</sup> for active particles<sup>87</sup> and for particles with discrete and stochastic ligand–receptor binding.<sup>88–90</sup> Specifically, the chemical and physical properties of the ligands have been investigated (*cf.* Fig. 4c).<sup>91</sup> For instance, simulations suggest that for longer ligands, initial membrane attachment is easier while full uptake becomes more difficult.

Particle wrapping not only deforms the adhered membrane parts, attached to the particle, but also the non-adhered free membrane parts, adjacent to the particle (*cf.* Fig. 4b). The two membrane parameters  $\kappa$  and  $\sigma$  define a length scale  $\lambda = \sqrt{\kappa/\sigma}$ , characterizing the deformations in the free membrane parts during uptake.<sup>75</sup> Using typical parameter values ( $\kappa = 25k_B T$  and  $\sigma = 10^{-5}–10^{-3} \text{ N m}^{-1}$ ) one finds  $\lambda = 10–100 \text{ nm}$ .<sup>90,92</sup> In order to characterize membrane deformations one considers the ratio  $\lambda/R$ , with  $R$  the particle radius, that determines how far deformations can penetrate into the free membrane parts.<sup>75,90,92</sup> For  $\lambda/R \ll 1$  we get a tense membrane where the deformation stays close to the particle, whereas for  $\lambda/R \gg 1$  we get a floppy membrane where the deformation reach is large. Inversely, the membrane parameters or the strength of adhesion can be predicted from the observation of the uptake state and the deformations of the membrane.

Apart from size and shape, the particle number affects the shape of membrane deformations during uptake.<sup>93,94</sup> If there are multiple particles present on the membrane, they can interact with each other through the deformations they induce, which can lead to an attractive interaction and the emergence of collective behavior.<sup>95–100</sup> Cooperative wrapping is a result of the interplay of bending and adhesion energy such that multiple wrapped particles can self-assemble into membrane tubes<sup>101</sup> linear aggregates,<sup>102</sup> hexagonal arrays<sup>103</sup> or rings.<sup>104</sup> In contrast, long parallel cylinders in globally flat membranes are predicted to repel each other.<sup>105</sup>

Some of these theoretical predictions on multiple-particle interactions on membranes still have to be confirmed by experimental studies, while others have been verified in recent years. These experiments typically involve giant lipid vesicles that wrap micrometer-sized particles because here membrane deformations are more easily accessible due to their larger sizes. For example this setup has been used to show that particles at membranes aggregate to reduce membrane deformations,<sup>98,106</sup>

assemble into 2D crystals with hexagonal order,<sup>107</sup> and to measure the state digram of wrapping in the tensionless regime.<sup>108</sup>

## 4.2 Clathrin-mediated endocytosis

Particle wrapping is often assisted by protein–membrane interactions and the assembly of protein superstructures, providing additional mechanisms to curve the membrane.<sup>109</sup> The most important example is clathrin-mediated endocytosis (CME).<sup>110</sup> In CME, clathrin triskelia with tripod shapes bind to membrane-embedded adaptor proteins, which leads to the formation of clathrin lattices (protein assemblies) at the cell membrane (*cf.* Fig. 4d). As a result of clathrin assembly, the membrane gets deformed and a clathrin-coated vesicle is created.<sup>111,112</sup> The sequence of assembly, membrane deformation and vesicle formation is regulated and before progression occurs several check-points have to be passed.<sup>112,113</sup> The timing of clathrin induced membrane deformations relative to the timing of lattice assembly, however, is still elusive and two models explaining the extreme cases of the invagination process exist: the constant curvature model and the constant area model.<sup>114,115</sup>

In the constant curvature model the clathrin coat grows with constant curvature, implying that the membrane is continuously deformed. In contrast, in the constant area model the clathrin coat first grows flat without curvature. Only after the coat has reached a sufficient size the membrane is deformed and a flat-to-curved transition occurs.<sup>110</sup> To transform a flat lattice into a curved clathrin coat, however, a topological barrier has to be overcome, since Euler's polyhedron criterion dictates that the number of faces and vertices minus the number of edges has to equal two for closed polyhedra. Therefore, twelve pentagons (or possibly more pentagons accompanied by equally many more heptagons) have to be incorporated into the otherwise hexagonal clathrin lattice.<sup>116,117</sup>

Assessing the assembly process of clathrin coats experimentally is difficult, because the involved length scales are below the diffraction limit, therefore standard light microscopy techniques cannot resolve the assembly process. However, significant steps have been taken in modeling and simulations. In order to investigate how clathrin coats deform the membrane, additional terms have been added to eqn (1), representing polymerization energy, line tension or bending energy of the clathrin coat.<sup>118–122</sup> In addition, simulations show how the assembly of clathrin triskelia deforms the membrane (*cf.* Fig. 4e and f).<sup>123,124</sup> The assembly of flat and invaginated clathrin lattices was suggested to result from triskelia which occur in a flat and curved configuration and from lattices that exhibit lattice vacancies.<sup>125,126</sup> The dynamics of clathrin coat assembly can be modeled by kinetic growth equations. A comparison of this model with the experimentally measured size and shape distribution of clathrin coated membranes suggests that clathrin coats first assemble flat before they start to curve.<sup>127</sup> However, it is still unresolved how this transition from flat to curved could take place precisely on a microscopic level.

While under normal conditions CME can occur without the contribution of polymerizing actin filaments, the situation changes if membrane tension is high, or for cells with turgor



pressure (e.g. yeast).<sup>130,131</sup> Now polymerizing actin filaments can prevent CME from being stalled and support the invagination process of a flat membrane into a curved vesicle.<sup>132,133</sup> It has been suggested by a combination of experiments and simulations that accessory proteins, triggering actin polymerization, organize in a ring-like manner around the endocytic site to optimize the efficiency of membrane invagination driven by actin<sup>134</sup> and that bent actin filaments contribute to internalization by releasing elastic energy upon getting straight.<sup>135</sup> To determine the rigidity of the clathrin coat and the force, generated by polymerizing actin filaments, in yeast cells, a shape equation, based on eqn (1), was fitted to registered membrane profiles.<sup>136</sup> Using this approach the rigidity of the clathrin coat and the generated force were determined to be between  $400\text{--}2000k_{\text{B}}T$  and  $1000\text{--}5000$  pN, respectively. It remains unclear, however, how and where the point force of the model, generated by the actin network, is exerted and distributed on the membrane (cell wall) in the cell.

### 4.3 Phagocytosis

Phagocytosis is the main pathway in which cells take up large particles ( $\geq 0.5 \mu\text{m}$ ) such as microbes (cf. Fig. 4g). For mammals the ability to phagocytose particles is mainly limited to immune cells to clear out pathogens, whereas single-cell organisms use it to take up nutrients.<sup>137–139</sup> Although the actual dynamics have not been fully resolved experimentally, phagocytosis can be modeled by a zipper mechanism, implying that phagocytosis is the collective interplay of many particle–membrane adhesion contacts. In detail, first particles adhere to the plasma membrane through sequential ligand–receptor binding. Second, the plasma membrane encloses the particle due to actin polymerization, which also leads to further ligand–receptor binding. Finally, the membrane fuses around the particle to enable the separation of the enveloped particle from the plasma membrane.<sup>137,139</sup>

In contrast to adhesion driven particle uptake, the particle size does not seem to play an important role for the effectiveness of phagocytosis,<sup>140</sup> suggesting that active processes are the dominant players involved. Indeed large particles are engulfed not just by the membrane but also by the growing actin cortex.<sup>128,139</sup> The polymerizing actin network leads to a particular type of membrane deformation, the so-called phagocytic cup, a membrane protrusion exhibiting increased membrane curvature since the membrane is deformed both in- and outwards.

Modeling the effect of ligand–receptor binding on the uptake dynamics suggests that the first half of engulfment is slow whereas the second half is fast.<sup>141</sup> Moreover, particle shape and orientation influences the uptake dynamics. For instance, oblate shaped particles are engulfed fastest when the flat surface is presented to the membrane first.<sup>142</sup> Surprisingly, for small particles phagocytosis has also been observed in systems where actin activity was inhibited, facilitated by ratcheted ligand–receptor binding alone, although the uptake rate is three to four times slower under such circumstances.<sup>128</sup> We note that the interpretation of this observation is still under debate.<sup>143</sup>

Actin polymerization renders the shape of the phagocytic cup more regular (cf. Fig. 4h). From the shape of phagocytic cup the necessary engulfment forces have been calculated.<sup>144</sup> The model predicts that two kinds of forces are at work: a repulsive force between the actin cytoskeleton and the membrane that leads to the engulfment of the particle and a flattening force that leads to the shape of the phagocytic cup. Furthermore, the shape and position of the phagocytic cup were investigated for a zymosan particle (made from yeast cell walls), where the membrane protrusion flows around the particle, leading to outward particle motion prior to engulfment, and for an antibody coated particle, where the membrane forms thin protrusions at all sides, leading to inward particle motion.<sup>129</sup> Simulations suggest that for the zymosan particle, the membrane is pushed by actin and does not adhere to the particle, whereas for the antibody coated particle, the membrane lacks protrusion and adheres to the particle (cf. Fig. 4i). Moreover, by observing the shapes of deformable hydrogel particles during phagocytosis with confocal microscopy, it is possible to calculate the tensile forces from the deformation of the particles.<sup>145</sup> Using this method, it was estimated that the cells exert a total tensile force of approximately 1 nN on the particle at the base of the phagocytic cup.

To conclude, modeling and observing endocytosis reveals amongst others how material properties of the membrane change the uptake behavior of particles and which particle shapes perform best, considering the uptake dynamics. Therefore, modeling could inform us on how to avoid undesirable uptake of harmful nanoparticles or pathogens but also which shapes should be used as potential drug carriers for therapeutical applications.

## 5 Cell adhesion

When a eukaryotic cell encounters a surface, it will spread upon and adhere to it, if the surface properties are favorable for the cell to form specific adhesion sites. The cell can also non-specifically interact with the surface, either by attractive Coulomb or van der Waals forces, or due to the repulsive effect of the glycocalyx (a cover of sugar molecules) and membrane fluctuations that both weaken the unspecific adhesion by electrostatic or steric (entropic) repulsion.<sup>146</sup>

The adhesion process along specific adhesion sites consists of multiple steps, in which the cell adapts to the changed environment, affecting both the plasma membrane and the cytoskeleton, and thus leading to dramatic cell shape changes.<sup>12</sup> In the first step, cell adhesion molecules or receptors, which are transmembrane proteins embedded in the plasma membrane, form bonds with ligands of the substrate or the extracellular matrix (ECM). Together, ligands and receptors work like lock-and-key. The most important protein family that conveys adhesion in humans are integrins, that bind to the corresponding ligands of the ECM, for example collagen or fibronectin.<sup>12,146</sup>

Due to the dynamic nature of cells, cell adhesion has to be a reversible process. Therefore, individual bonds are weak and contribute only a few  $k_{\text{B}}T$  of adhesion energy. However, an ensemble of many bonds provides sufficient energy to establish





strong cell–surface adhesion.<sup>12,146</sup> For instance, integrins can assemble into focal adhesions, which are supra-molecular adhesion sites that strongly couple the actin cytoskeleton to the ECM.

During the initial spreading phase of adhesion, the cell surface area increases by about 50% due to the formation of adhesion sites, while the volume of the cell remains constant.<sup>147</sup> The excess membrane area originates from wrinkles or exocytosis.<sup>148</sup> The area gain is actively driven because the plasma membrane is pushed outwards by polymerizing actin filaments, creating a branched and cross-linked network of actin filaments at the leading edge of the cell. Between adhesion sites, cells develop actin stress fibers, that can be contracted by molecular motors. The generated forces are then transmitted *via* focal adhesion to the substrate.

Fig. 5a and b show a schematic view of an adhering cell after the internal remodeling process. In side view, the cell is essentially flat with only the cell nucleus sticking out (Fig. 5a). In the top view, the shape of the cell is characterized by invaginated arcs that span between focal adhesions (Fig. 5b).

### 5.1 Adhesion of membrane patches

The starting point to model specific cell adhesion is usually a continuum approach. In the basic model a spherical vesicle interacts by adhesion energy with the substrate, similar to the description of particle uptake (*cf.* eqn (9)). By minimizing the energy, the equilibrium membrane shape is determined (*cf.* Fig. 5c).<sup>149</sup> The approach can be extended straightforwardly

to an adhered vesicle from which a tether is pulled.<sup>150</sup> Inversely, the adhesion energy density can be determined by fitting the shape equations to experimentally observed membrane contours.

Since cells specifically adhere to a substrate by forming discrete ligand–receptor bonds, the model can be improved by incorporating the discrete nature of the adhesion sites. Ligand–receptor bonds can be modeled as springs. The adhesion part of the energy functional (in the Monge gauge) then reads

$$\mathcal{H} = \int \sum_{k=1}^N \delta(\mathbf{r} - \mathbf{r}_k) \left\{ \frac{\zeta}{2} (h(\mathbf{r}) - l_0)^2 - \varepsilon \right\} d\mathbf{r}, \quad (10)$$

where  $\mathbf{r} = (x, y)$  is the position on the membrane,  $\zeta$  the spring stiffness,  $l_0$  the rest length,  $\varepsilon$  the bond energy and  $N$  the total number of receptors.<sup>146</sup> Together with the usual description for the membrane (*cf.* eqn (3)) membrane adhesion can be studied for instance by Monte Carlo simulations.<sup>151</sup> This approach allows to predict the domain patterns of bound receptors during immune cell adhesion. Alternatively, eqn (10) can be used to calculate a force acting on the membrane that can be combined with rates for receptor binding and unbinding (fulfilling detailed balance) and membrane fluctuation dynamics, as described by eqn (8), to get a Langevin equation for the height function of an adhering membrane.<sup>152,153</sup> Fig. 5d shows a snapshot of a simulated shape of such a fluctuating membrane that adheres to a surface by binding ligands to receptors. The model can predict the number of ligand–receptor bonds that are necessary to nucleate a stable adhesion domain and the corresponding nucleation time.

### 5.2 Shapes and contours of adherent cells

After a cell has spread, its shape is determined by the tension that acts on invaginated membrane arcs that span between focal adhesions (*cf.* Fig. 5b).<sup>154</sup> These arcs are especially prominent in cells cultured on patterned substrates,<sup>155,156</sup> as shown in Fig. 5e and f. Micropatterns then define adhesive and non-adhesive areas, regulating where and how cells adhere to surfaces.<sup>156,157</sup>

To model the membrane shapes of adherent cells on patterned substrates, continuum models, discrete network models and cell contour models are employed.<sup>158–162</sup> The basis of all contour models is the simple tension model, relating tensions within the cell contour to membrane deformations or cell shapes.<sup>12,155</sup> After spreading, the cell is essentially flat, hence, it is described as a surface bound within a contour  $\mathbf{r}(s)$ , that is parametrized by its arc length  $s$ . If the cell is in equilibrium, the contractile forces of the actin cytoskeleton locally balance the force of the actin cortex at the cell contour. In the model, the surface tension  $\sigma$  is then locally balanced by the line tension  $\lambda$  (*cf.* Fig. 5b, inset). A tangent  $\mathbf{t}(s)$  and a normal vector  $\mathbf{n}(s)$  are defined at any point of the contour. If both vectors are normalized they are related by  $d\mathbf{t}(s)/ds = \mathbf{n}(s)/R(s)$ , with  $R(s)$  the local radius of curvature. If  $\sigma$  and  $\lambda$  are independent of  $s$ , the force balance on a contour element  $ds$  can be expressed by

$$\sigma \mathbf{n}(s) ds = \lambda (\mathbf{t}(s + ds) - \mathbf{t}(s)), \quad (11)$$

where the left hand side represents the force, caused by the cytoskeleton, acting in normal direction on the contour, and

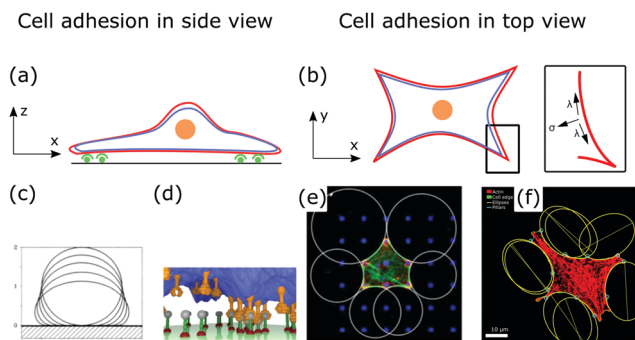


**Fig. 5** Membrane deformations in cell adhesion. (a) Schematic of cell adhesion in side view. A cell (nucleus: orange, membrane: red, actin cortex: blue) adheres to a surface at adhesion sites (green). (b) Schematic of cell adhesion in top view (nucleus: orange, membrane: red, actin cortex: blue). On patterned substrates cell shapes of adherent cells can be described by contour models. Inset: The contour of the cell shape can be described by the competition of surface and line tension. (c) Computed shapes of a membrane that adheres to a surface. By increasing the adhesion energy the contact area between membrane and surface increases. Reproduced from ref. 149 with permission from the American Physical Society, copyright (1990). (d) Simulated shape of a fluctuating membrane (blue) that adheres to a surface by binding receptors (orange) to ligands (grey). Reproduced from ref. 153 under the terms of the Creative Commons Attribution License (CC BY 3.0). (e) Theoretically predicted circular arcs fitted to the contour of adherent cells. Reproduced from ref. 155 with permission from Elsevier, copyright (2008). (f) Ellipses fitted to the contour of adherent cells. Reproduced from ref. 163 with permission from the American Physical Society, copyright (2018).



the right hand side represents the force that is caused by the actomyosin cortex at every point of the contour. Using the geometrical relation that connects  $\mathbf{t}(s)$  and  $\mathbf{n}(s)$ , eqn (11) leads to  $R = \lambda/\sigma$ . This expression resembles the Laplace law (cf. Section 2), but now in 2D. Fig. 5e shows circular arcs fitted to the contour of an adherent cell. The different radii show that the cortical tensions vary locally within the cell.

Alternatively, cell shapes can be described on the level of energies, connecting contour models with the framework derived for membrane shapes in Section 2. Similar to eqn (1), the energy functional then reads

$$\mathcal{H} = \sigma \int dA + \lambda \oint ds, \quad (12)$$

where the first term represents a surface tension energy and the second term represents a line tension energy.<sup>162</sup> The variation of eqn (12) leads to the same contour equation as before ( $R = \lambda/\sigma$ ). More advanced contour models also take the elasticity of the actin cortex (tension-elasticity model),<sup>155</sup> the bending rigidity of the membrane<sup>164</sup> or the anisotropy of the cytoskeleton (cf. Fig. 5f)<sup>163</sup> into account.

To conclude, modeling cell shape during cell adhesion contributes to our understanding of how the cytoskeletal network architecture and molecular motor contractility regulate cell shapes. Inversely, from observed cell shapes, especially on patterned surfaces, we can infer mechanical properties not just of the membrane, but also of the underlying cortical cytoskeleton.

## 6 Cell migration

Cell motility is another example of a cellular process where the plasma membrane is strongly deformed from the spherical reference state, affecting cell shape globally.<sup>165</sup> In general, cell motility can be classified into swimming motility and substrate-based motility, including cell gliding and crawling. For both swimmers and gliders the overall cell shape does not change much.<sup>166</sup> Thus, here, we focus on cell crawling where cell shape changes are most important, requiring continuous remodeling of the interior of the cell.<sup>167</sup>

The diversity of the shapes of migrating cells is huge and depends, among others, on the environment in which cells move. The same cell will assume vastly different shapes if it moves along a one-dimensional collagen fiber, a two-dimensional epithelial tissue, or through three-dimensional interstitial tissue.<sup>168</sup> The most common cell shapes that develop in cell crawling are lamellipodia (2D sheets of a branched actin network), filopodia (protrusions of parallel actin bundles), blebs (membrane bulges, driven by hydrostatic pressure and a weak connection to the actin cortex) and lobopodia (blunt protrusions, driven by hydrostatic pressure).<sup>169</sup>

The mechanism underlying lamellipodia based cell migration consists of several steps. First, cell polarity is established, *i.e.*, the front and back of the cell form. Second, the plasma membrane and the leading edge of the lamellipodium are pushed outwards through actin polymerization and branching.

The actin system is linked to the substrate at focal adhesions that form at the front and dissolve at the back of the cell. Therefore, traction forces are exerted to the substrate leading to forward motion of the cell. Finally, the back of the cell is pulled forwards because the actomyosin cytoskeleton contracts.<sup>169</sup> Thus, cell migration is achieved by constant internal remodeling of the cell causing steady shape changes (cf. Fig. 6a).

In the most basic model of cell migration, both the cell shape and the microscopic origins of motility are neglected and migration is described purely in terms of persistent random walks,<sup>170</sup> which is indeed observed for individual cells in a uniform environment. In a complementary approach, the interplay between cell migration, mediated through actin polymerization, and cell adhesion, mediated by stochastic linkers, has been theoretically studied recently. Focusing on the microscopic driving factors while still neglecting cell shape, it was found that the stick-slip dynamics of the traction force can explain both steady cell crawling and bipedal cell motion.<sup>171</sup>

A more detailed phenomenological approach is to reproduce the shape of different cell types in a rule-based “shape machine”, where different cell shapes can be generated by tuning model parameters that summarize many molecular interactions (cf. Fig. 6b).<sup>172,175</sup> For instance, one rule is that protrusions are formed at the leading edge whereas protrusions are suppressed anywhere else. By using cell shape as input information such models can make predictions about the internal structure of the cell. Results include the prediction that microtubule depolymerization increases the rate with which cells retract,<sup>172</sup> and a relation between the dynamics of the actin cytoskeleton, such as the capping rate and the stall force, and the observed shape of fish keratocytes.<sup>175</sup> Furthermore, computer simulations of the motion of flexocytes (vesicles with enclosed filaments) suggest that cell shape and the persistence of trajectories of migrating cells correlate.<sup>176</sup>

Another method to address the shape of migrating cells are cellular Potts models,<sup>173,177–179</sup> in which crawling cells are discretized on a lattice. Individual lattice sites can be added or removed from cells, allowing the cells to fluctuate and move over (simulation) time. Equilibrium configurations are typically determined from the minimization of an appropriate energy functional using Monte Carlo methods. Using such a model it was suggested that cell shape is not only a consequence of cellular signaling but also that these signaling processes are influenced by cell shape changes.<sup>177</sup> The approach can also be used to predict the shape of cells moving in ensembles (cf. Fig. 6c).<sup>173</sup>

Phase-field models are another approach to study cell migration.<sup>180</sup> The basic idea here is to represent the cell by a continuous field, the phase-field  $\rho$ , at the position  $r$  and time  $t$ , which is  $\rho = 1$  inside the cell, and  $\rho = 0$  outside the cell. Consequently, the cell membrane or interface of the cell is represented by a smooth change of the phase-field. Similar to eqn (1) the bending and tension energy of the cell membrane can be formulated in terms of the phase-field by<sup>180</sup>

$$\mathcal{H} = \frac{\kappa}{2} \int \frac{1}{\varepsilon} \left( \varepsilon \nabla^2 \rho - \frac{G'}{\varepsilon} \right)^2 dx dy + \sigma \int \left( \frac{\varepsilon}{2} |\nabla \rho|^2 + \frac{G}{\varepsilon} \right) dx dy, \quad (13)$$



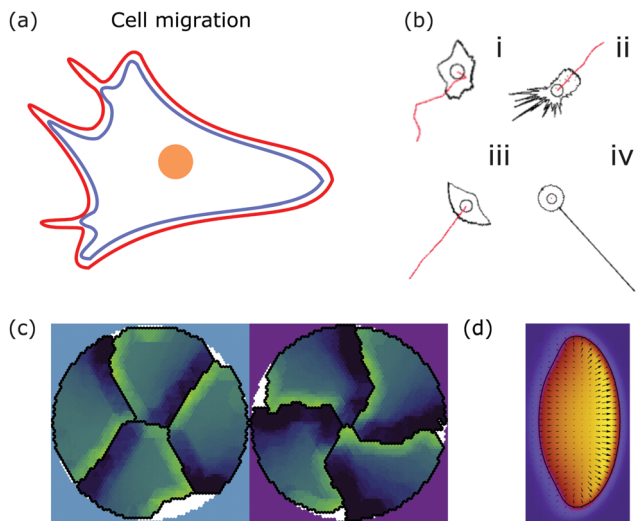


**Fig. 6** Membrane deformations in cell migration. (a) Schematic of a crawling cell (nucleus: orange, membrane: red, actin cortex: blue) that exhibits continuous internal remodeling affecting overall cell shape, including the lamellipodium and filopodia. (b) Phenomenological model that produces different cell shapes by changing the model parameters. Modeled cell shapes (black), paths of migration (red) and starting point of migration (black circle) for (i) dictyostelium cells, (ii) fibroblasts, (iii) keratocytes, and (iv) neurons. Reproduced from ref. 172 with permission from Elsevier, copyright (2008). (c) Shapes of four confined crawling cells modeled in a cellular Potts model. Reproduced from ref. 173 under the terms of the Creative Commons Attribution License (CC BY 4.0). (d) Crawling cell in the phase-field model. The heat map encodes the value of the phase-field from zero (purple) to one (yellow). Reproduced from ref. 174 with permission from The Royal Society of Chemistry.

where  $\varepsilon$  characterizes the interface width of  $\rho$  and  $G(\rho)$  is a function that interpolates between 0 and 1; a typical choice is  $G(\rho) = 18\rho^2(1 - \rho)^2$ .

From eqn (13) a line density force for bending and tension can be calculated by  $\mathbf{F}_{\text{ben}} + \mathbf{F}_{\text{ten}} = (\delta\mathcal{H}/\delta\rho)(\nabla\rho)/(\varepsilon|\nabla\rho|^2)$ . Adding contributions for area conservation  $\mathbf{F}_{\text{area}}$ , protrusion and retraction forces of actin filaments,  $\mathbf{F}_{\text{prot}}$  and  $\mathbf{F}_{\text{retr}}$ , and a friction force  $\mathbf{F}_{\text{fr}}$ , one finds the total force  $\mathbf{F}_{\text{tot}} = \mathbf{F}_{\text{ben}} + \mathbf{F}_{\text{ten}} + \mathbf{F}_{\text{area}} + \mathbf{F}_{\text{prot}} + \mathbf{F}_{\text{retr}} + \mathbf{F}_{\text{fr}}$ . At steady state there is no total force ( $\mathbf{F}_{\text{tot}} = 0$ ) and from  $\partial\rho/\partial t = \mathbf{v}\cdot\nabla\rho$ , with  $\mathbf{v}$  the local speed of the membrane or phase-field, the time evolution of the membrane follows as<sup>180</sup>

$$\begin{aligned} \tau \frac{\partial\rho}{\partial t} = & -\kappa \left( \nabla^2 - \frac{G''}{\varepsilon^2} \right) \left( \nabla^2\rho - \frac{G'}{\varepsilon^2} \right) + \sigma \left( \nabla^2\rho - \frac{G'}{\varepsilon^2} \right) \\ & - M_A \left( \int \rho dx dy - A_0 \right) |\nabla\rho| + (\alpha V - \beta W) |\nabla\rho|. \end{aligned} \quad (14)$$

In eqn (14)  $\tau$  characterizes the friction,  $A_0$  determines the prescribed cell area and  $M_A$  characterizes the strength of this area constraint. Moreover,  $V$  and  $W$  describe the concentration of cross-linked actin filaments and actin bundles, respectively, and  $\alpha$  and  $\beta$  characterize the protrusion and retraction forces. By solving eqn (14) together with the equations for the coupled fields  $V$  and  $W$ , the dynamics of the phase-field and thus the shape of the moving cell are determined.

Alternatively, the phase-field can be coupled to a vector field  $\mathbf{p}$ , describing polymerizing actin filaments.<sup>181</sup> Most importantly, the phase-field approach predicts the steady state shape of moving cells (*cf.* Fig. 6d).<sup>174,180,181</sup> Similar to the cellular Potts model the phase-field approach can be used to study the cell migration of cell ensembles.<sup>182</sup> In addition, it can be used to predict the shape of cells migrating in a 3D environment with different surface topographies.<sup>183</sup>

To conclude, theoretical modeling of cell migration reveals how driving factors on the molecular level regulate motility and shape changes on the cellular level. In addition, modeling shows how interactions between a cell and its environment affect shape dynamics, which can lead to emergent collective behavior with implications for wound healing and metastasis.

## 7 Cell division

From the viewpoint of shape, when animal cells divide, one sphere is transformed into two spheres, which fundamentally affects both the plasma membrane and the internal cellular components. To disentangle the underlying mechanisms cell division can be split up into multiple steps. In the first step, the cell rounds up and chromosomes assemble in the middle of the cell. In the second step, the chromosomes are pulled apart by mitotic spindles. In the third step, known as cytokinesis, the cell content is distributed between the two daughter cells.<sup>184,185</sup> Here we focus on symmetrical cytokinesis (*cf.* Fig. 7a).

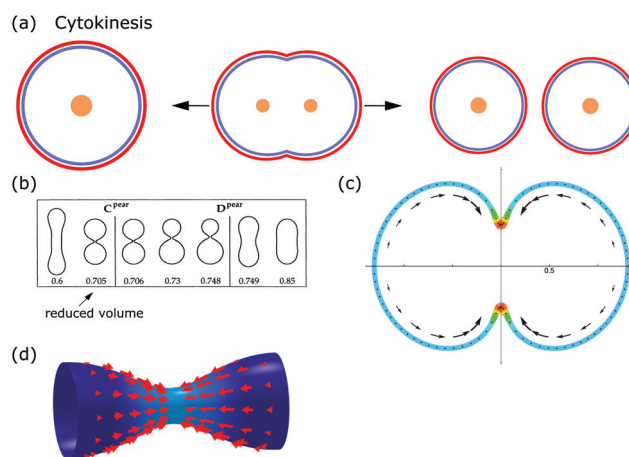


**Fig. 7** Membrane deformations in cell division. (a) Schematics of cytokinesis, the last step of cell division, where the cytoplasm is distributed over two daughter cells. Cell nucleus: orange, membrane: red, and actin cortex: blue. (b) Sequence of membrane shapes for constant spontaneous curvature and increasing reduced volume. Reproduced from ref. 31 with permission from the American Physical Society, copyright (1991). (c) Calculated cell shape during membrane constriction. The color code represents the activity within the cortex and the arrows show the cortical flow towards the equator. Reproduced from ref. 189 with permission from Elsevier, copyright (2014). (d) Shape of a constricting membrane tube due to the self-organizing flow of an active fluid (red arrows). Reproduced from ref. 190 under Creative Commons Attribution-NonCommercial-NoDerivatives License 4.0 (CC BY-NC-ND).



During cytokinesis the cellular volume  $V_0$  is conserved to a good approximation, *i.e.*  $V_0 = 2V_D$ , where  $V_D$  is the volume of a daughter cell.<sup>186</sup> Thus, by assuming spherical shapes it follows that  $2A_D \approx 1.26A_0$ , implying that the surface area of the daughter cells has to increase during cytokinesis. The necessary extra area is provided by exocytosis and membrane remodeling.<sup>23,187</sup> Moreover, the shape of the membrane changes drastically during cytokinesis. In order to model deformations of a cell of volume  $V$  and surface area  $A$ , one usually defines the reduced volume

$$\nu = \frac{V}{(4\pi/3)R_0^3}, \quad (15)$$

where  $R_0 = \sqrt{A/(4\pi)}$  is the radius of a sphere of the same surface area. While spherical shapes have  $\nu = 1$ , all other shapes have smaller values. In animal cells this shape change is driven by ATP-consuming activity within a ring of actomyosin that is anchored to the cell membrane, generating the necessary forces that constrict the membrane.<sup>188</sup>

From a physical point of view, the problem of cell division is similar to endocytosis, the main difference being that the parts created are the same size. Hence, the starting point for modeling cell division is again eqn (1). The membrane shapes, which are reminiscent of dividing cells, are then determined by solving the corresponding shape equation. One finds the sequence from spherical to splitting cells either by changing spontaneous curvature while keeping the reduced volume  $\nu$  constant, or by keeping spontaneous curvature constant while changing the reduced volume (*cf.* Fig. 7b).<sup>31</sup> Similar to this idea, a sequence of shapes reminiscent of dividing cells was found in a phase-field model as a result of a time-dependent spontaneous curvature.<sup>191</sup> Complementary, it has been demonstrated experimentally that vesicles could be split by changing their spontaneous curvature.<sup>192</sup>

Cell division in animal cells however is an active process, driven by the constriction of an actomyosin ring. Further details must therefore be included in the theoretical description.<sup>193</sup> From a conceptual point of view, probably the simplest way is to include the constriction force as a boundary condition at the midplane of the cell, and calculate the corresponding energy-minimizing shapes. However, these calculations suggest that symmetric division is unstable at constant volume.<sup>194,195</sup> The approach can be generalized to include the effect of membrane tension, spontaneous curvature and osmotic pressure.<sup>196,197</sup> A related approach is to represent the constriction force by a line tension energy, added to eqn (1). By fitting the solution of the corresponding shape equation to the shapes of dividing cells, the bending rigidity, the contractile force and the line tension could be determined.<sup>198</sup>

The models discussed above consider only the plasma membrane. These could be useful for the future development of artificial cells with a minimal internal structure. However, in animal cells the cytoskeleton cannot be neglected when considering large-scale changes. As a first step towards including the effects of the cytoskeleton, the contractile forces acting on the membrane can be modeled to originate from a gradient in

membrane tension during cytokinesis.<sup>199,200</sup> Building on this idea, cell shapes during cytokinesis were examined in a model that represents the composite of plasma membrane and actomyosin cortex as an active gel, which can restrict the initial spherical cell shape due to the internal activity within the gel.<sup>189</sup> A gradient in surface contractility from the poles to the equator then drives cytokinesis and, for example, reproduces the experimentally observed cortical flow to the equator (*cf.* Fig. 7c).

The constriction of the membrane can also be modeled by a contractile network that couples the network density with the spontaneous curvature of the membrane. In a framework similar to the one explained in Section 3 the dispersion and, hence, the stability of membrane constriction can be determined.<sup>201</sup> Moreover, the role of stress of different origins (adhesion, protrusion, contraction) acting on the membrane during cytokinesis has been investigated.<sup>202–204</sup>

As cytokinesis progresses, a cell–cell interface begins to form between the two daughter cells. The dynamics of this interface can be examined by balancing its viscous friction and active stresses. As a result, the model predicts the corresponding changes in cell shape.<sup>205</sup> Finally, curved surfaces can be coupled with active gels to study the interplay between different membrane shapes and contractile forces,<sup>190</sup> resulting for example in the formation of contractile rings on tubular membranes (*cf.* Fig. 7d).

To conclude, theoretical modeling of membrane deformations during cytokinesis predicts how membrane constriction might be initiated, how large constriction forces have to be and where they act. Therefore, modeling deformations in cell division contributes to our basic understanding necessary to build artificial cells.

## 8 Conclusion

The shape of the cell and the plasma membrane surrounding it are deformed in many cellular processes. The variety of the resulting membrane shapes shows the diversity of underlying driving factors. At the same time, this morphological variety allows us to extract a large amount of information about the inner workings of the cell. In this review we have outlined how modeling cell shape and membrane deformations can contribute to our understanding of the mechanisms that drive membrane fluctuations, endocytosis, cell adhesion, cell migration and cell division. We have demonstrated that modeling cell shape and membrane deformations is an important tool to investigate the cell, even on the microscopic scale.

The properties of a pure lipid bilayer membrane are well described by the Helfrich Hamiltonian (eqn (1)). Membrane deformations in a living cell however predominantly originate from active processes, which result in additional fluctuations, driven deformations, and large-scale shape and topological changes. To explain these shape changes, models can be built that include localized adhesion, changes in spontaneous curvature, or variation in stress, due to the interaction of the membrane with proteins and polymer networks. Inversely, the



calculated shapes can be fitted to experimental data to both verify the model predictions and extract material properties of the other cellular components involved, such as the magnitude of exerted forces or the adhesion energy of linker molecules.

In some cases, the experimental resolution in time or space is not yet high enough to distinguish between competing models, as for example in the two possible assembly pathways of a clathrin-coated pit discussed in section 4. While one of the proposed models might be ruled out by future experimental insight, it is also possible that both methods are employed. Life tends to be creative, and find a use for any pathway that is physically allowed, which is of course also why we can observe the large variety in membrane shapes we have explored here.

The discussed examples demonstrate how theoretical modeling can relate membrane deformations and shapes to cell function and thus lead to biological insight. In general, through modeling, the cell's complexity can be reduced and therefore modeling can identify key players, responsible for specific deformations. Moreover, modeling can couple theoretical concepts such as material parameters to observables such as fluctuation amplitudes or membrane invaginations, hence making the cell more quantifiable. Both these aspects show how theoretical modeling can reduce some of the cell's complexity by making predictions or hypotheses quantifiable.

We need not stop at the surface though. The insights we have gained about the inner workings of the cell by studying how it behaves in well-controlled situations like adhesion or phagocytosis allow us to also build models for more complex processes like cell migration and division. Because of the high complexity of cells, these models are by necessity more phenomenological; however, they can continually be refined as more detailed studies provide new information. Moreover, they provide a bridge from the fundamental study of lifeless components like lipid bilayers and proteins to full-fledged living cells, with promising applications in biology and medicine.

A well-known example is the difference between healthy and tumorigenic cells, which differ strongly in their material properties, allowing tumor cells to metastasize and invade healthy tissue. In this context, there is still a large array of questions to be answered, of which many center on the role of the membrane. For instance, while for reconstituted membranes or extracted membrane vesicles the membrane tension is uniform, recent experiments suggest that it is not in living cells.<sup>206</sup>

Recapitulating the different examples of this review, there are many more open questions to be answered. Membranes in living cells contain many different types of lipids, as well as transmembrane and membrane-associated proteins, which all affect membrane properties and shapes. There is still a large gap between experimentally reconstituted and theoretically modeled membranes with just a few, or just one component, and those we know to exist in living cells. Likewise, it is still quite elusive what the physiological role of active membrane fluctuations is. It is also still unknown what the minimal necessary requirements are for cells to divide, which might be especially important when engineering an artificial cell. Finally, there is a need to develop integrated models that bridge

multiple scales, for instance when studying the interplay between cell adhesion and cell migration.

To answer these questions, we need new experiments, but also new models, that take the interactions between the plasma membrane and cellular driving factors into account. More importantly, experimentalist and theorists need to continue working together, as these open questions can only be answered jointly.

## Conflicts of interest

There are no conflicts to declare.

## Acknowledgements

We thank Rachel Los, Ulrich Schwarz and Falko Ziebert for critical comments on the manuscript.

## References

- 1 B. Alberts, A. Johnson, J. Lewis, D. Morgan, M. Raff, K. Roberts and P. Walter, *Molecular biology of the cell: Sixth edition*, Garland Science, New York, 2015.
- 2 D. H. Boal, *Mechanics of the Cell*, Cambridge University Press, Cambridge, 2nd edn, 2012.
- 3 R. Phillips, J. Kondev, J. Theriot and H. Garcia, *Physical biology of the cell*, Garland Science, New York, 2012.
- 4 P. Schwille, J. Spatz, K. Landfester, E. Bodenschatz, S. Herminghaus, V. Sourjik, T. J. Erb, P. Bastiaens, R. Lipowsky, A. Hyman, P. Dabrock, J.-C. Baret, T. Vidakovic-Koch, P. Bieling, R. Dimova, H. Mutschler, T. Robinson, T.-Y. D. Tang, S. Wegner and K. Sundmacher, *Angew. Chem., Int. Ed.*, 2018, **57**, 13382–13392.
- 5 F. Fanalista, A. Birnie, R. Maan, F. Burla, K. Charles, G. Pawlik, S. Deshpande, G. H. Koenderink, M. Dogterom and C. Dekker, *ACS Nano*, 2019, **13**, 5439–5450.
- 6 Y. Mulla, A. Aufderhorst-Roberts and G. H. Koenderink, *Phys. Biol.*, 2018, **15**, 041001.
- 7 D. W. Thompson, *On Growth and Form*, Cambridge University Press, 1917.
- 8 A.-L. Le Roux, X. Quiroga, N. Walani, M. Arroyo and P. Roca-Cusachs, *Philos. Trans. R. Soc., B*, 2019, **374**, 20180221.
- 9 P. Bassereau and P. Sens, *Physics of Biological Membranes*, Springer, 2018.
- 10 L. Blanchoin, R. Boujemaa-Paterski, C. Sykes and J. Plastino, *Physiol. Rev.*, 2014, **94**, 235–263.
- 11 P. Chugh and E. K. Paluch, *J. Cell Sci.*, 2018, **131**, jcs186254.
- 12 U. S. Schwarz and S. A. Safran, *Rev. Mod. Phys.*, 2013, **85**, 1327–1381.
- 13 M. P. Clausen, H. Colin-York, F. Schneider, C. Eggeling and M. Fritzsche, *J. Phys. D: Appl. Phys.*, 2017, **50**, 064002.
- 14 F. Huber, A. Boire, M. P. López and G. H. Koenderink, *Curr. Opin. Cell Biol.*, 2015, **32**, 39–47.



- 15 S. Mostowy and P. Cossart, *Nat. Rev. Mol. Cell Biol.*, 2012, **13**, 183–194.
- 16 A. A. Bridges, M. S. Jentsch, P. W. Oakes, P. Occhipinti and A. S. Gladfelter, *J. Cell Biol.*, 2016, **213**, 23–32.
- 17 S. Banerjee, M. L. Gardel and U. S. Schwarz, *Annu. Rev. Condens. Matter Phys.*, 2020, **11**, 421–439.
- 18 M. Murrell, P. W. Oakes, M. Lenz and M. L. Gardel, *Nat. Rev. Mol. Cell Biol.*, 2015, **16**, 486–498.
- 19 S. Ramaswamy, *Annu. Rev. Condens. Matter Phys.*, 2010, **1**, 323–345.
- 20 M. C. Marchetti, J.-F. Joanny, S. Ramaswamy, T. B. Liverpool, J. Prost, M. Rao and R. A. Simha, *Rev. Mod. Phys.*, 2013, **85**, 1143.
- 21 M. R. Shaebani, A. Wysocki, R. G. Winkler, G. Gompper and H. Rieger, *Nat. Rev. Phys.*, 2020, **2**, 181–199.
- 22 H. Turlier and T. Betz, *Annu. Rev. Condens. Matter Phys.*, 2019, **10**, 213–232.
- 23 F. Rizzelli, M. G. Malabarba, S. Sigismund and M. Mapelli, *Open Biol.*, 2020, **10**, 190314.
- 24 W. Helfrich, *Z. Naturforsch., C: J. Biosci.*, 1973, **28**, 693–703.
- 25 M. Deserno, *Chem. Phys. Lipids*, 2015, **185**, 11–45.
- 26 S. Svetina and B. Žekš, *Eur. Biophys. J.*, 1989, **17**, 101–111.
- 27 S. Svetina and B. Žekš, *Anat. Rec.*, 2002, **268**, 215–225.
- 28 L. Miao, U. Seifert, M. Wortis and H.-G. Döbereiner, *Phys. Rev. E: Stat. Phys., Plasmas, Fluids, Relat. Interdiscip.*, 1994, **49**, 5389–5407.
- 29 O.-Y. Zhong-can and W. Helfrich, *Phys. Rev. A: At., Mol., Opt. Phys.*, 1989, **39**, 5280–5288.
- 30 R. Lipowsky, *Nature*, 1991, **349**, 475–481.
- 31 U. Seifert, K. Berndl and R. Lipowsky, *Phys. Rev. A: At., Mol., Opt. Phys.*, 1991, **44**, 1182–1202.
- 32 H. W. Gerald Lim, M. Wortis and R. Mukhopadhyay, *Proc. Natl. Acad. Sci. U. S. A.*, 2002, **99**, 16766–16769.
- 33 T. Baumgart, S. Das, W. W. Webb and J. T. Jenkins, *Biophys. J.*, 2005, **89**, 1067–1080.
- 34 S. Semrau, T. Idema, L. Holtzer, T. Schmidt and C. Storm, *Phys. Rev. Lett.*, 2008, **100**, 088101.
- 35 I. Derényi, F. Jülicher and J. Prost, *Phys. Rev. Lett.*, 2002, **88**, 238101.
- 36 T. R. Powers, G. Huber and R. E. Goldstein, *Phys. Rev. E: Stat., Nonlinear, Soft Matter Phys.*, 2002, **65**, 12.
- 37 P. Bassereau, B. Sorre and A. Lévy, *Adv. Colloid Interface Sci.*, 2014, **208**, 47–57.
- 38 F. Brochard and J. Lennon, *J. Phys.*, 1975, **36**, 1035–1047.
- 39 A. Biswas, A. Alex and B. Sinha, *Biophys. J.*, 2017, **113**, 1768–1781.
- 40 S. E. Lux, *Blood*, 2016, **127**, 187–199.
- 41 H. Duwe, J. Kaes and E. Sackmann, *J. Phys.*, 1990, **51**, 945–961.
- 42 T. Betz and C. Sykes, *Soft Matter*, 2012, **8**, 5317–5326.
- 43 H.-G. Döbereiner, G. Gompper, C. K. Haluska, D. M. Kroll, P. G. Petrov and K. A. Riske, *Phys. Rev. Lett.*, 2003, **91**, 048301.
- 44 H. Turlier, D. A. Fedosov, B. Audoly, T. Auth, N. S. Gov, C. Sykes, J.-F. Joanny, G. Gompper and T. Betz, *Nat. Phys.*, 2016, **12**, 513–519.
- 45 U. Seifert, *Adv. Phys.*, 1997, **46**, 13–137.
- 46 W. Helfrich and R.-M. Servuss, *Il Nuovo Cimento D*, 1984, **3**, 137–151.
- 47 J. Prost and R. Bruinsma, *Europhys. Lett.*, 1996, **33**, 321–326.
- 48 J. Prost, J.-B. Manneville and R. Bruinsma, *Eur. Phys. J. B*, 1998, **1**, 465–480.
- 49 L. C.-L. Lin and F. L. H. Brown, *J. Chem. Theory Comput.*, 2006, **2**, 472–483.
- 50 R. Granek and S. Pierrat, *Phys. Rev. Lett.*, 1999, **83**, 872–875.
- 51 S. Ramaswamy, J. Toner and J. Prost, *Phys. Rev. Lett.*, 2000, **84**, 3494–3497.
- 52 N. Gov, *Phys. Rev. Lett.*, 2004, **93**, 268104.
- 53 L. C.-L. Lin, N. Gov and F. L. H. Brown, *J. Chem. Phys.*, 2006, **124**, 074903.
- 54 B. Loubet, U. Seifert and M. A. Lomholt, *Phys. Rev. E: Stat., Nonlinear, Soft Matter Phys.*, 2012, **85**, 031913.
- 55 J.-B. Fournier, D. Lacoste and E. Raphaél, *Phys. Rev. Lett.*, 2004, **92**, 018102.
- 56 C. Dubus and J.-B. Fournier, *Europhys. Lett.*, 2006, **75**, 181–187.
- 57 R. Alert, J. Casademunt, J. Brugués and P. Sens, *Biophys. J.*, 2015, **108**, 1878–1886.
- 58 R. Zhang and F. L. H. Brown, *J. Chem. Phys.*, 2008, **129**, 065101.
- 59 N. S. Gov and A. Gopinathan, *Biophys. J.*, 2006, **90**, 454–469.
- 60 R. Shlomovitz and N. S. Gov, *Phys. Rev. Lett.*, 2007, **98**, 168103.
- 61 A. Maitra, P. Srivastava, M. Rao and S. Ramaswamy, *Phys. Rev. Lett.*, 2014, **112**, 258101.
- 62 C. Monzel and K. Sengupta, *J. Phys. D: Appl. Phys.*, 2016, **49**, 243002.
- 63 J.-B. Manneville, P. Bassereau, D. Lévy and J. Prost, *Phys. Rev. Lett.*, 1999, **82**, 4356–4359.
- 64 M. D. E. A. Faris, D. Lacoste, J. Pécréaux, J.-F. Joanny, J. Prost and P. Bassereau, *Phys. Rev. Lett.*, 2009, **102**, 038102.
- 65 T. Betz, M. Lenz, J.-F. Joanny and C. Sykes, *Proc. Natl. Acad. Sci. U. S. A.*, 2009, **106**, 15320–15325.
- 66 Y. Park, C. A. Best, T. Auth, N. S. Gov, S. A. Safran, G. Popescu, S. Suresh and M. S. Feld, *Proc. Natl. Acad. Sci. U. S. A.*, 2010, **107**, 1289–1294.
- 67 Y. Park, M. Diez-Silva, G. Popescu, G. Lykotrafitis, W. Choi, M. S. Feld and S. Suresh, *Proc. Natl. Acad. Sci. U. S. A.*, 2008, **105**, 13730–13735.
- 68 S. C. Takatori and A. Sahu, *Phys. Rev. Lett.*, 2020, **124**, 158102.
- 69 H. R. Vutukuri, M. Hoore, C. Abaurrea-Velasco, L. van Buren, A. Dutto, T. Auth, D. A. Fedosov, G. Gompper and J. Vermant, *Nature*, 2020, **586**, 52–56.
- 70 S. Zhang, H. Gao and G. Bao, *ACS Nano*, 2015, **9**, 8655–8671.
- 71 P. Cossart and A. Helenius, *Cold Spring Harbor Perspect. Biol.*, 2014, **6**, a016972.
- 72 L. Shang, K. Nienhaus and G. Nienhaus, *J. Nanobiotechnol.*, 2014, **12**, 5.



- 73 T. Wiegand, M. Fratini, F. Frey, K. Yserentant, Y. Liu, E. Weber, K. Galior, J. Ohmes, F. Braun, D.-P. Herten, S. Boulant, U. S. Schwarz, K. Salaita, E. A. Cavalcanti-Adam and J. P. Spatz, *Nat. Commun.*, 2020, **11**, 32.
- 74 S. Dasgupta, T. Auth, N. Gov, T. Satchwell, E. Hanssen, E. Zuccala, D. Riglar, A. Toyé, T. Betz, J. Baum and G. Gompper, *Biophys. J.*, 2014, **107**, 43–54.
- 75 M. Deserno, *Phys. Rev. E: Stat., Nonlinear, Soft Matter Phys.*, 2004, **69**, 031903.
- 76 Z. A. McDargh, P. Vázquez-Montejo, J. Guven and M. Deserno, *Biophys. J.*, 2016, **111**, 2470–2480.
- 77 M. Deserno and W. M. Gelbart, *J. Phys. Chem. B*, 2002, **106**, 5543–5552.
- 78 H. Gao, W. Shi and L. B. Freund, *Proc. Natl. Acad. Sci. U. S. A.*, 2005, **102**, 9469–9474.
- 79 R. Vácha, F. J. Martinez-Veracoechea and D. Frenkel, *Nano Lett.*, 2011, **11**, 5391–5395.
- 80 S. Dasgupta, T. Auth and G. Gompper, *Soft Matter*, 2013, **9**, 5473–5482.
- 81 S. Dasgupta, T. Auth and G. Gompper, *Nano Lett.*, 2014, **14**, 687–693.
- 82 R. Lipowsky and H.-G. Döbereiner, *Europhys. Lett.*, 1998, **43**, 219–225.
- 83 C. Huang, Y. Zhang, H. Yuan, H. Gao and S. Zhang, *Nano Lett.*, 2013, **13**, 4546–4550.
- 84 X. Yi, X. Shi and H. Gao, *Phys. Rev. Lett.*, 2011, **107**, 098101.
- 85 C. Zeng, M. Hernando-Pérez, B. Dragnea, X. Ma, P. van der Schoot and R. Zandi, *Phys. Rev. Lett.*, 2017, **119**, 038102.
- 86 J. Agudo-Canalejo and R. Lipowsky, *ACS Nano*, 2015, **9**, 3704–3720.
- 87 P. Chen, Z. Xu, G. Zhu, X. Dai and L.-T. Yan, *Phys. Rev. Lett.*, 2020, **124**, 198102.
- 88 X. Yi and H. Gao, *Nanoscale*, 2017, **9**, 454–463.
- 89 F. Frey, F. Ziebert and U. S. Schwarz, *Phys. Rev. Lett.*, 2019, **122**, 088102.
- 90 F. Frey, F. Ziebert and U. S. Schwarz, *Phys. Rev. E*, 2019, **100**, 052403.
- 91 H.-M. Ding and Y.-G. Ma, *Biomaterials*, 2012, **33**, 5798–5802.
- 92 L. Foret, *Eur. Phys. J. E: Soft Matter Biol. Phys.*, 2014, **37**, 42.
- 93 A. Chaudhuri, G. Battaglia and R. Golestanian, *Phys. Biol.*, 2011, **8**, 046002.
- 94 A. H. Bahrami, M. Raatz, J. Agudo-Canalejo, R. Michel, E. M. Curtis, C. K. Hall, M. Gradzielski, R. Lipowsky and T. R. Weikl, *Adv. Colloid Interface Sci.*, 2014, **208**, 214–224.
- 95 M. Goulian, R. Bruinsma and P. Pincus, *Europhys. Lett.*, 1993, **22**, 145–150.
- 96 B. J. Reynwar, G. Illya, V. A. Harmandaris, M. M. Müller, K. Kremer and M. Deserno, *Nature*, 2007, **447**, 461–464.
- 97 A. Šarić and A. Cacciuto, *Soft Matter*, 2013, **9**, 6677.
- 98 C. van der Wel, A. Vahid, A. Šarić, T. Idema, D. Heinrich and D. J. Kraft, *Sci. Rep.*, 2016, **6**, 32825.
- 99 A. Vahid, A. Šarić and T. Idema, *Soft Matter*, 2017, **13**, 4924–4930.
- 100 T. Idema and D. J. Kraft, *Curr. Opin. Colloid Interface Sci.*, 2019, **40**, 58–69.
- 101 A. H. Bahrami, R. Lipowsky and T. R. Weikl, *Phys. Rev. Lett.*, 2012, **109**, 188102.
- 102 A. Šarić and A. Cacciuto, *Phys. Rev. Lett.*, 2012, **109**, 188101.
- 103 A. Šarić and A. Cacciuto, *Phys. Rev. Lett.*, 2012, **108**, 118101.
- 104 A. Vahid and T. Idema, *Phys. Rev. Lett.*, 2016, **117**, 138102.
- 105 M. M. Müller, M. Deserno and J. Guven, *Phys. Rev. E: Stat., Nonlinear, Soft Matter Phys.*, 2005, **72**, 061407.
- 106 C. van der Wel, D. Heinrich and D. J. Kraft, *Biophys. J.*, 2017, **113**, 1037–1046.
- 107 M. Wang, A. M. Mihut, E. Rieloff, A. P. Dabkowska, L. K. Månsson, J. N. Immink, E. Sparr and J. J. Crassous, *Proc. Natl. Acad. Sci. U. S. A.*, 2019, **116**, 5442–5450.
- 108 H. T. Spanke, R. W. Style, C. François-Martin, M. Feofilova, M. Eisentraut, H. Kress, J. Agudo-Canalejo and E. R. Dufresne, *Phys. Rev. Lett.*, 2020, **125**, 198102.
- 109 J. Zimmerberg and M. M. Kozlov, *Nat. Rev. Mol. Cell Biol.*, 2006, **7**, 9–19.
- 110 M. Kaksonen and A. Roux, *Nat. Rev. Mol. Cell Biol.*, 2018, **19**, 313.
- 111 A. Picco and M. Kaksonen, *Curr. Opin. Cell Biol.*, 2018, **53**, 105–110.
- 112 M. Mettlen, P.-H. Chen, S. Srinivasan, G. Danuser and S. L. Schmid, *Annu. Rev. Biochem.*, 2018, **87**, 871–896.
- 113 R. T. Pedersen, J. E. Hassinger, P. Marchando and D. G. Drubin, *J. Cell Biol.*, 2020, **219**, e202002160.
- 114 M. Lampe, S. Vassilopoulos and C. Merrifield, *J. Struct. Biol.*, 2016, **196**, 48–56.
- 115 K. A. Sochacki and J. W. Taraska, *Trends Cell Biol.*, 2019, **29**, 241–256.
- 116 R. J. Mashl and R. F. Bruinsma, *Biophys. J.*, 1998, **74**, 2862–2875.
- 117 T. Kohyama, D. M. Kroll and G. Gompper, *Phys. Rev. E: Stat., Nonlinear, Soft Matter Phys.*, 2003, **68**, 061905.
- 118 R. Lipowsky, *J. Phys. II*, 1992, **2**, 1825–1840.
- 119 A. Banerjee, A. Berezhkovskii and R. Nossal, *Biophys. J.*, 2012, **102**, 2725–2730.
- 120 M. Saleem, S. Morlot, A. Hohendahl, J. Manzi, M. Lenz and A. Roux, *Nat. Commun.*, 2015, **6**, 6249.
- 121 J. E. Hassinger, G. Oster, D. G. Drubin and P. Rangamani, *Proc. Natl. Acad. Sci. U. S. A.*, 2017, **114**, E1118–E1127.
- 122 F. Frey and U. S. Schwarz, *Soft Matter*, 2020, **16**, 10723–10733.
- 123 R. Matthews and C. N. Likos, *Soft Matter*, 2013, **9**, 5794.
- 124 M. Giani, W. K. den Otter and W. J. Briels, *J. Chem. Phys.*, 2017, **146**, 155102.
- 125 W. K. den Otter and W. J. Briels, *Traffic*, 2011, **12**, 1407–1416.
- 126 F. Frey, D. Bucher, K. A. Sochacki, J. W. Taraska, S. Boulant and U. S. Schwarz, *New J. Phys.*, 2020, **22**, 073043.
- 127 D. Bucher, F. Frey, K. A. Sochacki, S. Kummer, J.-P. Bergeest, W. J. Godinez, H.-G. Kräusslich, K. Rohr, J. W. Taraska and U. S. Schwarz, *et al.*, *Nat. Commun.*, 2018, **9**, 1109.
- 128 S. Tollis, A. E. Dart, G. Tzircotis and R. G. Endres, *BMC Syst. Biol.*, 2010, **4**, 149.
- 129 M. Herant, C.-Y. Lee, M. Dembo and V. Heinrich, *PLoS Comput. Biol.*, 2011, **7**, e1001068.



- 130 S. Boulant, C. Kural, J.-C. Zeeh, F. Ubelmann and T. Kirchhausen, *Nat. Cell Biol.*, 2011, **13**, 1124–1131.
- 131 L. Johannes, R. G. Parton, P. Bassereau and S. Mayor, *Nat. Rev. Mol. Cell Biol.*, 2015, **16**, 311–321.
- 132 A. E. Carlsson, *Curr. Opin. Cell Biol.*, 2018, **50**, 1–7.
- 133 F. Baschieri, K. Porshneva and G. Montagnac, *J. Cell Sci.*, 2020, **133**, jcs240861.
- 134 M. Mund, J. A. van der Beek, J. Deschamps, S. Dmitrieff, P. Hoess, J. L. Monster, A. Picco, F. Nédélec, M. Kaksonen and J. Ries, *Cell*, 2018, **174**, 884–896. e17.
- 135 M. Akamatsu, R. Vasan, D. Serwas, M. A. Ferrin, P. Rangamani and D. G. Drubin, *eLife*, 2020, **9**, e49840.
- 136 S. Dmitrieff and F. Nédélec, *PLoS Comput. Biol.*, 2015, **11**, e1004538.
- 137 J. A. Swanson, *Nat. Rev. Mol. Cell Biol.*, 2008, **9**, 639–649.
- 138 D. M. Richards and R. G. Endres, *Rep. Prog. Phys.*, 2017, **80**, 126601.
- 139 V. Jaumouillé and C. M. Waterman, *Front. Immunol.*, 2020, **11**, 1097.
- 140 J. A. Champion and S. Mitragotri, *Proc. Natl. Acad. Sci. U. S. A.*, 2006, **103**, 4930–4934.
- 141 D. M. Richards and R. G. Endres, *Biophys. J.*, 2014, **107**, 1542–1553.
- 142 D. M. Richards and R. G. Endres, *Proc. Natl. Acad. Sci. U. S. A.*, 2016, **113**, 6113–6118.
- 143 V. Heinrich, *Biophys. J.*, 2015, **109**, 469–476.
- 144 M. Herant, *J. Cell Sci.*, 2006, **119**, 1903–1913.
- 145 D. Vorselen, Y. Wang, M. M. de Jesus, P. K. Shah, M. J. Footer, M. Huse, W. Cai and J. A. Theriot, *Nat. Commun.*, 2020, **11**, 20.
- 146 K. Sengupta and A.-S. Smith, *Physics of Biological Membranes*, Springer, 2018, pp. 499–535.
- 147 N. C. Gauthier, O. M. Rossier, A. Mathur, J. C. Hone and M. P. Sheetz, *Mol. Biol. Cell*, 2009, **20**, 3261–3272.
- 148 N. C. Gauthier, M. A. Fardin, P. Roca-Cusachs and M. P. Sheetz, *Proc. Natl. Acad. Sci. U. S. A.*, 2011, **108**, 14467–14472.
- 149 U. Seifert and R. Lipowsky, *Phys. Rev. A: At., Mol., Opt. Phys.*, 1990, **42**, 4768–4771.
- 150 A.-S. Smith, E. Sackmann and U. Seifert, *Phys. Rev. Lett.*, 2004, **92**, 208101.
- 151 T. R. Weikl, M. Asfaw, H. Kroboth, B. Rózycki and R. Lipowsky, *Soft Matter*, 2009, **5**, 3213.
- 152 T. Bühr, U. Seifert and A.-S. Smith, *Phys. Rev. Lett.*, 2012, **109**, 258101.
- 153 T. Bühr, U. Seifert and A.-S. Smith, *New J. Phys.*, 2015, **17**, 083016.
- 154 R. Bar-Ziv, T. Tlusty, E. Moses, S. A. Safran and A. Bershadsky, *Proc. Natl. Acad. Sci. U. S. A.*, 1999, **96**, 10140–10145.
- 155 I. B. Bischofs, F. Klein, D. Lehnert, M. Bastmeyer and U. S. Schwarz, *Biophys. J.*, 2008, **95**, 3488–3496.
- 156 P. J. Albert and U. S. Schwarz, *Cell Adhes. Migr.*, 2016, **10**, 516–528.
- 157 C. S. Chen, *Science*, 1997, **276**, 1425–1428.
- 158 S. Banerjee and M. Cristina Marchetti, *New J. Phys.*, 2013, **15**, 035015.
- 159 V. S. Deshpande, R. M. McMeeking and A. G. Evans, *Proc. Natl. Acad. Sci. U. S. A.*, 2006, **103**, 14015–14020.
- 160 M. F. Coughlin and D. Stamenović, *Biophys. J.*, 2003, **84**, 1328–1336.
- 161 P. Guthardt Torres, I. B. Bischofs and U. S. Schwarz, *Phys. Rev. E: Stat., Nonlinear, Soft Matter Phys.*, 2012, **85**, 011913.
- 162 L. Giomi, *Cell Migrations: Causes and Functions*, Springer, Cham, 2019, pp. 13–29.
- 163 W. Pomp, K. Schakenraad, H. E. Balcioğlu, H. van Hoorn, E. H. J. Danen, R. M. H. Merks, T. Schmidt and L. Giomi, *Phys. Rev. Lett.*, 2018, **121**, 178101.
- 164 S. Banerjee and L. Giomi, *Soft Matter*, 2013, **9**, 5251.
- 165 A. Mogilner and K. Keren, *Curr. Biol.*, 2009, **19**, R762–R771.
- 166 D. A. Fletcher and J. A. Theriot, *Phys. Biol.*, 2004, **1**, T1–T10.
- 167 P. Sens and J. Plastino, *J. Phys.: Condens. Matter*, 2015, **27**, 273103.
- 168 V. te Boekhorst, L. Preziosi and P. Friedl, *Annu. Rev. Cell Dev. Biol.*, 2016, **32**, 491–526.
- 169 D. L. Bodor, W. Pönisch, R. G. Endres and E. K. Paluch, *Dev. Cell*, 2020, **52**, 550–562.
- 170 D. Selmeczi, L. Li, L. I. Pedersen, S. F. Nrrrelykke, P. H. Hagedorn, S. Mosler, N. B. Larsen, E. C. Cox and H. Flyvbjerg, *Eur. Phys. J.-Spec. Top.*, 2008, **157**, 1–15.
- 171 P. Sens, *Proc. Natl. Acad. Sci. U. S. A.*, 2020, 202011785.
- 172 J. Satulovsky, R. Lui and Y.-l. Wang, *Biophys. J.*, 2008, **94**, 3671–3683.
- 173 F. Thüroff, A. Goychuk, M. Reiter and E. Frey, *eLife*, 2019, **8**, e46842.
- 174 J. Löber, F. Ziebert and I. S. Aranson, *Soft Matter*, 2014, **10**, 1365–1373.
- 175 K. Keren, Z. Pincus, G. M. Allen, E. L. Barnhart, G. Marriott, A. Mogilner and J. A. Theriot, *Nature*, 2008, **453**, 475–480.
- 176 C. Abaurrea-Velasco, T. Auth and G. Gompper, *New J. Phys.*, 2019, **21**, 123024.
- 177 A. F. M. Maré, V. A. Grieneisen and L. Edelstein-Keshet, *PLoS Comput. Biol.*, 2012, **8**, e1002402.
- 178 P. J. Albert and U. S. Schwarz, *Biophys. J.*, 2014, **106**, 2340–2352.
- 179 F. Zhou, S. A. Schaffer, C. Schreiber, F. J. Segerer, A. Goychuk, E. Frey and J. O. Rädler, *PLoS One*, 2020, **15**, e0230679.
- 180 D. Shao, W.-J. Rappel and H. Levine, *Phys. Rev. Lett.*, 2010, **105**, 108104.
- 181 F. Ziebert, S. Swaminathan and I. S. Aranson, *J. R. Soc., Interface*, 2012, **9**, 1084–1092.
- 182 J. Löber, F. Ziebert and I. S. Aranson, *Sci. Rep.*, 2015, **5**, 9172.
- 183 B. Winkler, I. S. Aranson and F. Ziebert, *Commun. Phys.*, 2019, **2**, 82.
- 184 J. G. Carlton, H. Jones and U. S. Eggert, *Nat. Rev. Mol. Cell Biol.*, 2020, **21**, 151–166.
- 185 R. A. Green, E. Paluch and K. Oegema, *Annu. Rev. Cell Dev. Biol.*, 2012, **28**, 29–58.
- 186 J. Sedzinski, M. Biro, A. Oswald, J.-Y. Tinevez, G. Salbreux and E. Paluch, *Nature*, 2011, **476**, 462–466.





- 187 M. Fürthauer and M. González-Gaitán, *Cell Cycle*, 2009, **8**, 3311–3318.
- 188 A. L. Miller, *Curr. Biol.*, 2011, **21**, R976–R978.
- 189 H. Turlier, B. Audoly, J. Prost and J.-F. Joanny, *Biophys. J.*, 2014, **106**, 114–123.
- 190 A. Mietke, F. Jülicher and I. F. Sbalzarini, *Proc. Natl. Acad. Sci. U. S. A.*, 2019, **116**, 29–34.
- 191 R. A. Barrio, T. Alarcon and A. Hernandez-Machado, *PLoS One*, 2020, **15**, e0227562.
- 192 J. Steinkühler, R. L. Knorr, Z. Zhao, T. Bhatia, S. M. Bartelt, S. Wegner, R. Dimova and R. Lipowsky, *Nat. Commun.*, 2020, **11**, 905.
- 193 D. B. Cortes, A. Dawes, J. Liu, M. Nickaen, W. Strychalski and A. S. Maddox, *J. Cell Sci.*, 2018, **131**, jcs203570.
- 194 V. G. Almendro-Vedia, F. Monroy and F. J. Cao, *PLoS One*, 2013, **8**, e69750.
- 195 V. G. Almendro-Vedia, F. Monroy and F. J. Cao, *Phys. Rev. E: Stat., Nonlinear, Soft Matter Phys.*, 2015, **91**, 012713.
- 196 E. Beltrán-Heredia, V. G. Almendro-Vedia, F. Monroy and F. J. Cao, *Front. Physiol.*, 2017, **8**, 312.
- 197 E. Beltrán-Heredia, F. Monroy and F. J. Cao-García, *Phys. Rev. E*, 2019, **100**, 052408.
- 198 H. Koyama, T. Umeda, K. Nakamura, T. Higuchi and A. Kimura, *PLoS One*, 2012, **7**, e31607.
- 199 H. Greenspan, *J. Theor. Biol.*, 1977, **65**, 79–99.
- 200 J. White and G. Borisy, *J. Theor. Biol.*, 1983, **101**, 289–316.
- 201 R. Shlomovitz and N. S. Gov, *Biophys. J.*, 2008, **94**, 1155–1168.
- 202 C. C. Poirier, W. P. Ng, D. N. Robinson and P. A. Iglesias, *PLoS Comput. Biol.*, 2012, **8**, e1002467.
- 203 J. F. Dorn, L. Zhang, T.-T. Phi, B. Lacroix, P. S. Maddox, J. Liu and A. S. Maddox, *Mol. Biol. Cell*, 2016, **27**, 1286–1299.
- 204 J. Zhao and Q. Wang, *Int. J. Numer. Methods Biomed. Eng.*, 2016, **32**, e02774.
- 205 A. Sain, M. M. Inamdar and F. Jülicher, *Phys. Rev. Lett.*, 2015, **114**, 048102.
- 206 Z. Shi, Z. T. Graber, T. Baumgart, H. A. Stone and A. E. Cohen, *Cell*, 2018, **175**, 1769–1779. e13.

